Nano-Plasmonics: a stepping stone into Non-linear Quantum Plasmonics

Rúben Azinheira Alves
Mestrado Integrado em Engenharia Física
Departamento de Física e Astronomia
2017

Orientador
Prof. Dr. Ariel Guerreiro, Faculdade de Ciências

U.PORTO

FACULDADE DE CIÊNCIAS
UNIVERSIDADE DO PORTO

Todas as correções determinadas pelo júri, e só essas, foram efetuadas.

O Presidente do Júri,

Porto, _____/_____/_____

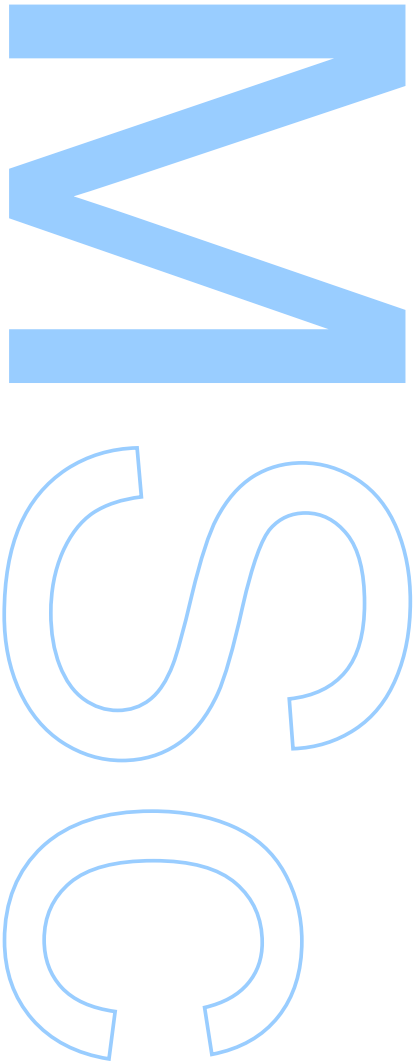

UNIVERSIDADE DO PORTO

MASTERS THESIS

Nano-Plasmonics: a stepping stone into Non-linear Quantum Plasmonics

Author:
Rúben ALVES

Supervisor:
Ariel GUERREIRO

A thesis submitted in fulfilment of the requirements
for the degree of Master of Science

at the

Faculdade de Ciências
Departamento de Física e Astronomia

October 2017

" I am and always will be the optimist, the hoper of far-flung hopes and the dreamer of improbable dreams "

Matt Smith as *The Doctor*, written by Matthew Graham

Acknowledgements

First and foremost I would like to thank my supervisor, Prof. Dr. Ariel Guerreiro, and Nuno Azevedo Silva for their enthusiasm, guidance and constant support throughout the development of this thesis. Without them this project wouldn't be possible.

I would also like to express my gratitude to everyone in the Centre for Applied Photonics of INESC-TEC. Because of them I was able to work for the first time in a professional environment.

Without a doubt I am grateful to everyone in PHYSIKUP - Núcleo de Física, Engenharia Física e Astronomia, in particular to my colleague and co-founder Sofia Ferreira Teixeira, we managed to create something that hopefully will improve our department.

I owe my heartfelt gratitude to my colleagues and esteemed friends Rita Lima, João Costa, Miguel Gomes and Regina Magalhães for all their patience, motivation and bullying. Without their every day help and friendship I wouldn't reach this point. They taught me how to study and for that I will be forever grateful. To my friends Pedro Leal and João Marques for all those game nights (and days) and talks that sometimes extended far beyond the reasonable. Also to Inês Cruz and Carlos Nunes for all those "just a coffee" nights out up until 8 am. I will never forget all the moments we passed together.

To my childhood friends Ana Oliveira, Angelo Borges and Pedro Rodrigues, I am thankful for all those Saturday nights during which I would endlessly rant about physics even though they most likely would have rather talked about something else.

I will be forever thankful to my family, my mother for all her motherly patience and love that only a mother can have, to my father that taught me to always ask questions despite the fact he eventually had to answer them and to my sister for making my life much harder in a way that only a younger sister can, I am very proud of you. I love you all very much.

Finally I would like to thank every one that has challenged me one way or the other, because of them, intentional or not, I was able to grow while overtaking them.

UNIVERSIDADE DO PORTO

Abstract

Faculdade de Ciências
Departamento de Física e Astronomia

Master of Science

Nano-Plasmonics: a stepping stone into Non-linear Quantum Plasmonics

by Rúben ALVES

This thesis investigates the new phenomena exhibited by plasmons in nano-scale structures and their analogy with systems and models of Quantum Mechanics and Non-linear Physics in order to explore new optical sensing principles. Indeed, when plasmons are strongly confined near the surface of a metal they are affected by the refractive index of the surrounding media. This has provided the fundamental principle for a whole generation of optical sensors that lasted for several decades, with increasing sensitivity and sophistication.

Recent developments in fabrication techniques have pushed the confinement of plasmons even further into nano-scale structures (such as nano-wires, dimers, nano-spheres, among others). At these scales plasmons can exhibit new and exotic properties, such as non-linear and quantum effects, capable of supporting new sensing principles. This thesis aims to provide a steeping stone towards capturing this new technological potential by proposing new models (both conceptual and numerical) and providing a deeper insight into this new frontier of plasmonics. As a demonstration of the possibilities opened by nano-plasmonic sensing, it is presented a proposal for an electrostatic field sensor based on these models and perspectives.

UNIVERSIDADE DO PORTO

Resumo

Faculdade de Ciências
Departamento de Física e Astronomia

Mestrado em Engenharia Física

Nano-Plasmónica: um passo em direcção à Plasmónica Quântica Não-Linear

por Rúben ALVES

Esta tese investiga um novo fenómeno demonstrado por plasmões à nano-escala e, a analogia entre os modelos e sistemas encontrados em Mecânica Quântica e Física Não-linear para explorar novos princípios em sensores ópticos. Quando plasmões estão confinados na superfície de um metal, são fortemente afectados pelo índice de refracção do meio circundante. Este princípio, que elevou a sensibilidade e sofisticação, foi a base para toda uma geração de sensores ópticos que durou várias décadas.

Desenvolvimentos recentes nas técnicas de fabricação fizeram com que o confinamento de plasmões fosse maior até uma barreira foi atingida na nano-escala. Nestas escalas os plasmões podem demonstrar novas e exóticas propriedades como não-linearidades e efeitos quânticos, capazes de suportar novos princípios físicos para sensores. Esta tese ambiciona fornecer um patamar para que este novo potencial tecnológico seja alcançado, propondo novos modelos (conceptuais e numéricos) e proporcionando um melhor entendimento desta nova fronteira da Plasmónica, tais como uma demonstração das possibilidades de sensores baseados em nano-plasmónica e, uma proposta de um sensor de campo eléctrico estático baseado nestes modelos e perspectivas.

Contents

List of Figures

Chapter 1

Introduction

One of the most interesting topics in optical sensing today is the understanding of how the non-linear and quantum aspects of localized plasmons in nano-scale structures can be used not only to improve the sensing performance, but also to provide new sensing approaches. However, the implications of this research problem extend well beyond sensing to many other technological applications and physical insights into the interaction between light and matter.

The fields of Photonics and Plasmonics are two of cutting edge technologies of the early 21st century that are hoped to overcome the limitations of Electronics, the dominant technology of the end of the 20th century. While Photonics is the science and technology of generating, controlling, and detecting photons, Plasmonics focuses on the study of the interaction between electromagnetic field and free electrons in materials, typically metals. One of the strongest point of electronic technologies is the ability to downscale devices and their components to scales ranging from some hundreds to a few tens of nanometres. On the other hand, photonic devices can yield much faster data transference rates, far in excess of several Gigahertz. Indeed, one of the most accomplished photonic devices is the optical fibre that allows fast telecommunications and data transmissions, a device that today is used worldwide. The public demand for increasing performance resulted in the development of devices continuously decreased in size to replace the semiconductor-based electronics, while maintaining a superior operation speed. Photonic devices are however bounded by a fundamental barrier common to all dielectric wave-guides: the diffraction limit. This implies that light cannot be confined to dimensions smaller than half its wavelength. Plasmonics emerged as a possible solution for this limitation since it relies on the strong coupling between free electrons and light. Indeed, Plasmonics can

be thought as a hybrid between Electronics and Photonics as it retains the high-speed data transference of photonic devices [3] while allowing to go beyond the diffraction limit into devices the size of semiconductor electronics [4], therefore providing a combination between the advantages of both. This is ilustrated in Figure 1.1.

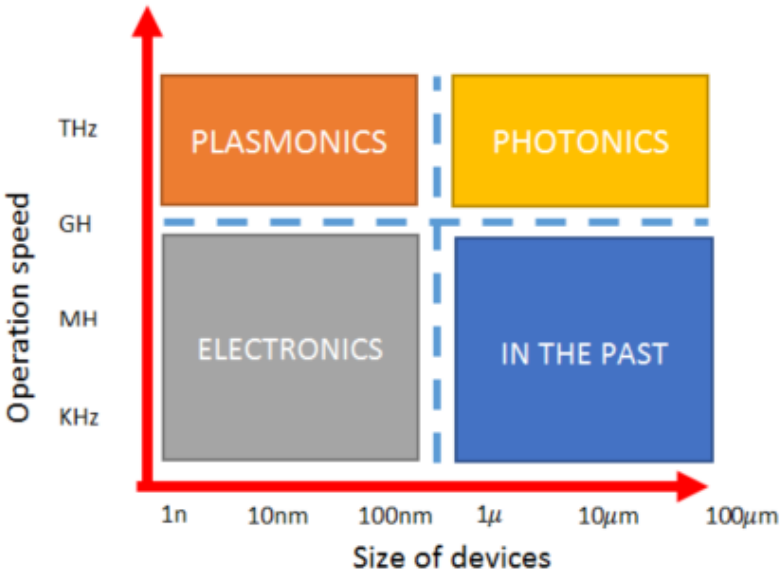

FIGURE 1.1: Technology domains characterized by their feature size and operation speed.

Although computer chips based on Plasmonics might still be some years away, there is already some work that shows promise [5]. In the past few decades, Plasmonics evolved optical sensing tremendously with the development of technologies based on the surface plasmon resonance that already have commercial applications. However and in the long run, the importance of Plasmonic goes beyond sensing since it constitutes a testing ground that allows to solve particular technical challenges (from fabrication to dissipation control) that might support the future replacement of semiconductor technologies.

1.1 State of the Art

Historically, the term "Plasmon" was first used in 1956 to describe a quanta of the collective electronic oscillation in a plasma discharge, which was very similar to electronic oscillations in solids [6]. A Plasmon can be considered as a quasi-particle defined as a collective oscillation of conduction electrons in materials excited by electromagnetic radiation. They normally occur in metals but can also be found in some semi-conductors [7]. The nature of plasmons often exhibits strong non-linear effects not only in terms of

their optical properties [8] but also in terms of the dynamics of the electrons [9], specially when confined to scales bellow of a few tens or hundreds of nanometres. Plasmons are typically understood as a macroscopic phenomena involving a number of particles higher than 10^{30}, occurring at high temperatures. However, can Plasmons exhibit a quantum aspect?

Plasmons in condensed matter are typically divided into two groups [10], on one hand we find the volume or bulk plasmons that are charged oscillations propagating through the interior of material domains [11], while on the other hand we find the surface plasmons which can only propagate in the interface between two media if certain special conditions are fulfilled [12].

The study of plasmons is a very rich field, not only in terms of the fundamental physics associated with the interaction of light and matter in continuous media, but also for the myriad of applications that have emerged in the past decades and are expected to be developed in the near future. One of the first great technological success of plasmonics is in the high sensitivity in optical sensing [13], but it is also necessary to mention particular achievements such as sub-wavelength focussing [14], the development of some types of optical meta-materials [15], among others. All these achievements have provided know-how in the control and application of plasmons but there is still many challenges to overcome when we attempt to downscale the material structures that support plasmons to the nano-scale. This miniaturization process is expected to further increase the sensitivity of optical sensors, allowing the replacement of electronics with a new generation of information technologies applying sophisticated effects associated with the control of light.

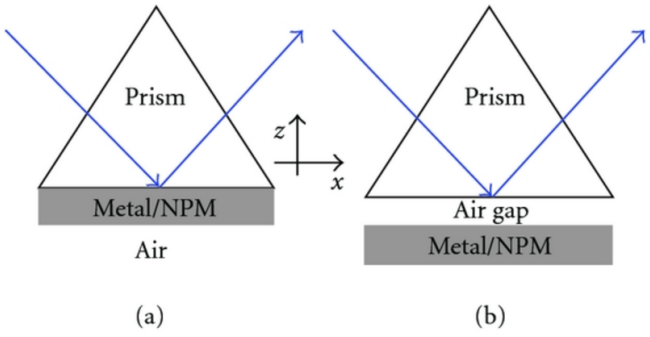

FIGURE 1.2: a) The Kretschmann configuration. b) The Otto configuration.

In the case of optical sensing the first breakthrough at the basis of the current technological application of Plasmonics can be traced back to 1968, when Otto and Krestchmann & Raether devised two possible configuration to excite a plasmon in a metal. In the Otto configuration, light illuminates a prism in the condition of total internal reflection then, a thin metal film is positioned in the vicinity of the prism, but still with a gap of air, so that the evanescent wave in the inner surface of the metal interacts with the metal thus exciting the plasmon. In contrast, in the Kretschmann configuration the metal film is evaporated directly onto the prism, which allows light to travel through the prism, penetrate in the metal film as an evanescent wave, and excite surface plasmons in the outer side of the film. Figure 1.2 show the difference between the two setups.

The basic treatment of light scattering by metals was predominantly set in the first decades of the 1900's, even before the term Plasmon was introduced. The Drude Model of free electrons in 1900 [16] and the Mie's theory for the scattering and absorption of electromagnetic radiation by a sphere in 1908 [17], still form the theoretical background of most of the papers published on Surface Plasmons. However, with the evolution of nano-fabrication techniques, it has been possible to develop structures with dimensions of a few hundreds of nanometres which strongly confine the motion of the electrons inside the metal, giving rise to a new type of Plasma oscillations known as Localised Surface Plasmons [18].

These localized surface plasmons can produce even stronger interactions between light and matter that can further improve the sensing performance. However, there are many aspects of plasmons localized in nano-metric structures that need to be addressed, both from a fundamental and from an experimental perspective. It is therefore not surprising the continuous interest of research in these topics, expressed by the continuous increase of publications dedicated to plasmonics, as one can see in Fig 1.3. In particular, this interest has prompt new models and new descriptions of plasmons at the nano-scale and ultimately the quantum behaviour of plasmons at these small scales.

Recently, it was introduced the Hydrodynamical Model that describes the plasmons in a material as a fluid of charge coupled with the electromagnetic field [19]. The main advantages of this model are that it takes into account atomic and subatomic interactions [20], in particular electron-electron repulsion by considering the Pauli Exclusion Principle, that forbids two fermions from occupying the same quantum state at a given time [21]. Unfortunately, this description looks at plasmons as classical objects, and does not take

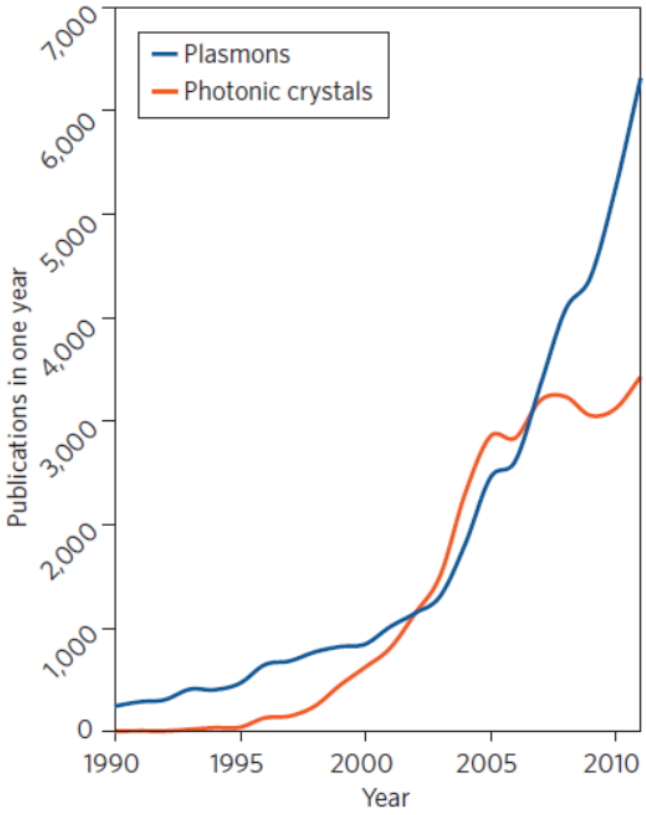

FIGURE 1.3: Number of publications in plasmonics (Blue) and in photonic crystals (Orange) [1]

into account the possibility that the plasmons can be a quantum phenomena.

Indeed, there are many reasons why plasmons should not exhibit quantum properties as they are a collective effect involving more than 10^{30} charged particles. Although, Bulk and Surface plasmons are mainly classical in nature, localised surface plasmons have been demonstrated experimentally to have a quantum character. For example by studying the entanglement of photon-plasmon-photon [22–24], quantum tunnelling [25, 26] and even sub-wavelength confinement in meta-materials and graphene [27]. However, some authors have attempted to provide a quantum model for plasmons by studying and experimenting each properties independent from each other, like entanglement [28], decoherence and loss [29], quantum size confinement [30], among others, this is essential if one wants to, someday, reach a complete quantum model for plasmons.

As one can see, a full quantum description of plasmonic systems is required. However, to reach that objective, one has to introduce a description based on a quantum many-body approach. For this, there are two distinct models: the Hartree-Fock approximation and the Density Functional Theory.

The Hartree-Fock approximation has provided the starting point for many quantum many-body theories by finding an effective single-particle Hamiltonian that can be diagonalized and whose ground-state can be used as an approximation to the true ground-state of the whole system [31]. This approximation is based on the Slater determinant that provides an expression of the wave function of a multi-fermionic system that satisfies the Pauli exclusion principle and can be used to compute the ground state for an N-body electron plasmonic system.

The concept of Density Functional Theory describes the whole system in terms of the electronic density without the explicit reference to the many-body wave function. The aim of this theory is to minimize the energy as a functional of the density. Although this may seem ideal, the effective potential characterized has a local response in space and a non-local dependence on the density and therefore can only be viewed as an approximation [31]. Much like the Hartree-Fock approximation, one could use this theory to describe and solve an N-body electron plasmonic system.

1.2 Structure of the thesis

This Thesis is divided in 6 chapters. The first chapter introduces the topic, provides the state of the art and the outputs achieved during the course of this thesis. Chapter 2 provides the models to describe plasmons in metallic structures. This chapter starts with the classical model for plasmons, where the Maxwell equations are presented then proceeds to show the Drude model for free electrons and the Lorentz oscillator model. It is possible to apply these models on metal nano-structures, such as thin films, nano-wires and nano-spheres. This chapter ends presenting the semi-classical model, the hydrodynamical Drude model, in association with the Madelung formalism.

Following the hydrodynamical Drude model in association with the Madelung formalism one has to solve a non-linear Schrödinger equation. In chapter 3 one presents a possible approximation for this equation linearising it. This chapter shows the numerical method used as well as the result obtained. On the other hand, chapter 4 provides the numerical method used to solve the non-linear Schrödinger equation and the results while comparing them with the ones obtained previously.

Chapter 5 starts with some theoretical background of the Rabi oscillations and, subsequently, presents a design and operation principles of an optical sensor based on fibre optics and plasmonics where the models developed in this thesis are applied.

Chapter 6 provides some conclusions and possible future work.

1.3 Outputs

During the course of this thesis, the author has contributed to the following outputs:

- 12 conference papers, of which 3 as first author;
- 2 oral presentations;
- 12 poster presentations, of which 3 as first author.

The first author publication were:

- R. A. Alves, Nuno A. Silva, J. C. Costa, M. Gomes and A. Guerreiro, "The Analogue Quantum Mechanical of Plasmonic Atoms",Proc. SPIE 10453, Third International Conference on Applications of Optics and Photonics, 1045314 (22 August 2017) ;
- R. A. Alves, Nuno A. Silva, J. C. Costa, M. Gomes and A. Guerreiro, "Doppler Broadening Effects in Plasmonic Quantum Dots", Proc. SPIE 10453, Third International Conference on Applications of Optics and Photonics, 1045316 (22 August 2017);
- R. A. Alves, J. C. Costa, M. Gomes, Nuno A. Silva, J. L. Santos and A. Guerreiro, "Quantum Wires as Sensors of the electric Field: A model into Quantum Plasmonics" 25th international Conference on Optical Fiber Sensors (23 April 2017).

Chapter 2

Physical Model

The treatment of plasmons, describing the coupling between light and the charge oscillation in materials such as metals and semiconductors, has evolved tremendously over the past few years as the structures that support these quasi-particles become smaller, reaching today scales of the order of the nanometre [32]. At these scales, the properties of plasmons are quite exotic due, not only to confinement effects, but also the fact that charged particles in the material and light itself exhibit their quantum nature [33]. Additionally, as the size of the structures that support plasmons decreases, the light pulse used to excite the plasmons also decreases reaching scales of a few picoseconds. At these durations transient effects also affect the properties of plasmons, which contrasts with the classical models used less than a decade ago nonetheless, these models are still used to describe phenomena and are applied in a wide range of scientific fields ranging from bionanotechnology [34] to optical sensing [35, 36].

The level of detail used to describe plasmons is determined not only by the physical properties of the systems that support them, but also by the effort to make these descriptions as simple as possible while keeping them useful. In fact, plasmons are strongly non-linear collective phenomena, that include the dynamics of charges in the media under the influence of an electromagnetic component.

From the point of view of the charges, the system is described by a quantum many body problem characterized by a complicated wave-function involving the position and velocity of all the charges [23]. From the point of view of the electromagnetic field, it involves the distribution of light intensity throughout the material and its different refractive index [37]. It is this last approach that is commonly used in the early description

of plasmons. However, as the technology and fabrication techniques evolve, and non-linear quantum plasmonics becomes a reality [26], the description of plasmons must take into account these dimensions to attain an adequate model of these phenomena.

This chapter provides a review of different models for plasmons. In Section 2.1 one looks at the early description of plasmons that focus on the electromagnetic component and is followed a classical approach. The next section provides examples to obtain the optical modes for metallic micro to nano films, wires and spheres. In this description the material properties are considered stationary, thus one can neglect the transient effects and describe the systems in terms of refractive index. Section 2.3 presents a more detailed description where the charges of the material are described as a fluid that responds to the field. This description is able to account for confinement effects in the scale of a few nanometres and some quantum features, such as the Thonmas - Fermi pressure.

2.1 The Classical Model for Plasmons

This section will provide the models needed to understand the classical treatment for plasmonics discussed in the next section. Subsection 2.1.1 discusses the Maxwell equation, followed by 2.1.2 where some of the material's properties are described. In subsection 2.1.3 the Drude model is presented and finally, subsection 2.1.4 provides the Lorentz Oscillator model.

2.1.1 Maxwell Equations

The classical model of plasmons describes the electromagnetic field with classical electrodynamics based on the macroscopic Maxwell equations. Although plasmons are usually defined as the quanta of oscillations of the charge density of a material, this phenomena has a classical electromagnetic counterpart. As charges oscillate, their collective motion breaks the local charge equilibrium, producing an electromagnetic field that forces the restoration of charge neutrality. As a result, during a charge oscillation of the plasmon, the kinetic energy of the electrons is converted into potential energy stored in the field and vice versa. The classical description of plasmons is developed on top of this classical electromagnetic counterpart of a plasmon, in terms of the macroscopic Maxwell equations, where the behaviour and response of the charges are included as the optical properties of the material, namely the macroscopic susceptibility. This set of equations assume the

statistical average of the electric and magnetic field. This is taken over an infinitesimal volume, that has to be smaller than the wavelength of the field and yet, larger than the mean inter-atomic interaction distance. In doing so, one can consider only the macroscopic response of the medium. With that in mind, one can start by stating the Maxwell equations

$$\nabla \times \vec{E} = -\frac{\partial \vec{B}}{\partial t} \tag{2.1}$$

$$\nabla \cdot \vec{D} = \rho_{ext} \tag{2.2}$$

$$\nabla \times \vec{H} = \vec{J}_{ext} + \frac{\partial \vec{D}}{\partial t} \tag{2.3}$$

$$\nabla \cdot \vec{B} = 0, \tag{2.4}$$

where $\vec{D}$ is the dielectric displacement field, $\vec{E}$ is the electric field, $\vec{H}$ is the magnetic field and $\vec{B}$ is the magnetic induction field [38].

One should note that the field vectors $\vec{D}$ and $\vec{B}$ are defined as

$$\vec{D} = \varepsilon_0(1+\chi)\vec{E} = \varepsilon_0 \boldsymbol{\varepsilon} \vec{E} \tag{2.5}$$

and

$$\vec{B} = \mu_0 \boldsymbol{\mu} \vec{H}, \tag{2.6}$$

where χ, $\boldsymbol{\varepsilon}$ and $\boldsymbol{\mu}$ are the susceptibility tensor, the electric permittivity tensor and the magnetic permeability tensor, respectively, ε_0 and μ_o are the vacuum electric permittivity and the vacuum magnetic permeability. As most of the diamagnetic and paramagnetic metals lose their magnetic properties early, before reaching the optical range, it will be assumed that the magnetic permeability tensor ($\boldsymbol{\mu}$) is the identity matrix.

2.1.2 Material Properties

When accounting the interaction of an electromagnetic field with a metal, one usually separates the charge carriers of the metal into two types: *quasi-free* conduction electrons and bound charges, being the last a subsystem composed of the bond between electrons and nuclei. These two types of charge carriers have their own mobilities and the interaction with the electromagnetic field will be different. Therefore, one writes the contributions to the metal's susceptibility as

$$\chi(\omega) = \chi_{free}(\omega) + \chi_{bound}(\omega) \tag{2.7}$$

and its permittivity as

$$\varepsilon(\omega) = 1 + \chi_{free}(\omega) + \chi_{bound}(\omega), \tag{2.8}$$

where χ_{free} and χ_{bound} are the susceptibilities of the free electrons and the subsystem of the bound charge carriers. For a clear definition of χ_{bound}, one should use *ab initio* a fully quantum mechanical approach, however in doing so, a N-body Schrödinger equation has to be solved consistently with Maxwell's equations in the presence of a surface. Although, a normal plasmonic system is of the order of a few hundred nanometres, it comprises billions of atoms and the sheer scale of the problem effectively limits the fully quantum mechanical approach to the simplest of models. Also, the contribution from the free or conduction electrons must be calculated using empirical data or effective models that provide a simplified description of plasmons. The following sections describe some of the most common of such models.

2.1.3 Drude Model

The Drude Model is an application of the Kinetic Theory of gases, where it is assumed that the atomic nuclei of the metal are static and that the electrons of a metal are gas molecules that obey the equation

$$\partial_t \vec{p} = q\left(\vec{E} + \frac{\vec{p} \times \vec{B}}{m}\right) - \frac{\vec{p}}{\tau}, \tag{2.9}$$

where $\vec{p}$, q, m and τ are the electron's momentum, charge, mass and the mean time between ionic collisions, respectively.

Despite the limitations of this model, it is usually the first model studied when learning solid state physics. This model predicts an electric permittivity given by

$$\varepsilon(\omega) = 1 - \frac{\omega_p^2}{\omega^2 + i\gamma\omega}, \tag{2.10}$$

where $\omega_p = \sqrt{\frac{Ne^2}{m_e \varepsilon_0}}$ is the plasma frequency.

Although this model is purely classic and empirical, it provides a good description of the response of metals below the energy of electronic inter-band transitions.

2.1.4 The Lorentz Oscillator Model

As it was previously stated, the bound charge contribution should be practically impossible to determine without using a fully quantum model. However, there is one purely

classical model that provides a simple picture and basic insight into the light-matter interaction: the Lorentz oscillator. This model assumes that the subsystem of a bound electron-nucleus can be described as an oscillator, where the electron moves around the nucleus with the characteristic frequency given by the band gap of the material. Then, the subsystem of all the bound charges can be comprised of a number N of such oscillators with their own frequency $\omega_i \neq 0$. By applying a time dependent electric field, the interaction between said field and the oscillators should result in a polarization given by

$$\vec{P}_b = \sum_{i=1}^{N} \vec{P}_i, \tag{2.11}$$

where $\mathbf{P}_i$ obeys the differential equation

$$\frac{\partial^2 \mathbf{P}_i}{\partial t^2} + \gamma_i \frac{\partial \mathbf{P}_i}{\partial t} + \omega_i^2 \mathbf{P}_i = \frac{\Omega_i^2}{4\pi} \mathbf{E}, \tag{2.12}$$

with these equations one can find the susceptibility of bound charges of the Lorentz model as

$$\chi_b(\omega) = \sum_{t=1}^{N} \chi_i(\omega), \tag{2.13}$$

where $\chi_i(\omega)$ is given by the following relation

$$\chi_i(\omega) = \frac{\Omega_i^2}{\omega_i^2 - \omega^2 - i\gamma_i\omega}. \tag{2.14}$$

As it was stated, this model is purely classical, however it is widely used for fitting experimental measures especially if the imaginary component of χ_b is composed of a single symmetric peak.

2.2 Plasmons in metal films and nano-structures

The previous models comprise all the theoretical knowledge needed to describe plasmonics in terms of the Maxwell equations, where the response of the electron density is contained in the susceptibility. This description is sufficient when describing bulk plasmons. However, when modelling surface and localized plasmons it is necessary to consider the contribution of the geometry of the metal to the dispersion relation. For surface and localized plasmons the boundary conditions imposed by the shape of the metal films or nano-strutures determine the plasmonic modes, and ultimately their dispersion relation.

This section investigates the structure of plasmon in thin films and nano-strutures, from nano-wires to nano-spheres. The study of plasmons in confined geometries typically results in a discrete spectrum of the plasmon modes, similar to the spectrum of the solutions to the Schrödinger equation in a potential box. This represents the first step in the development of a quantum description of plasmons.

2.2.1 Plasmons in a thin film

For the description of surface plasmons in a planar waveguide, one presents an electromagnetic theory of optical waveguides based on solving the Maxwell equations using the modal method [10]. This approach assumes that a dielectric waveguide is placed between two dielectric layers. After reaching the dispersion relation, one assumes that the electric permittivity is represented by a complex number which is characteristic of metals.

This means that the electric field and the magnetic field are of the form

$$\vec{E}(\vec{r},t) = \vec{E}_G(\vec{r},t) + \vec{E}_R(\vec{r},t) \tag{2.15}$$

$$\vec{H}(\vec{r},t) = \vec{H}_G(\vec{r},t) + \vec{H}_R(\vec{r},t), \tag{2.16}$$

where subscript G and R denote the guided and the radiation fields. The guided fields can be expressed as a finite sum of the guided modes such as

$$\vec{E}_G(\vec{r},t) = \sum_j \alpha_j \vec{E}_j(\vec{r},t) \tag{2.17}$$

$$\vec{H}_G(\vec{r},t) = \sum_j \alpha_j \vec{H}_j(\vec{r},t), \tag{2.18}$$

where j is the mode number and α_j are the modal amplitudes. One can easily conclude that Eqs. (2.15) and (2.16) are solutions to the source-free Maxwell equations.

Assuming that the waveguide is a linear isotropic media, one can reduce the Maxwell equations to

$$\Delta\vec{E}(\vec{r},t) - \varepsilon_0\varepsilon(\vec{r})\mu_0\frac{\partial^2\vec{E}(\vec{R},t)}{\partial t^2} = \nabla(\vec{E}(\vec{r},t)\cdot\nabla\ln\varepsilon_0\varepsilon(\vec{r})) \tag{2.19}$$

$$\Delta\vec{H}(\vec{r},t) - \varepsilon_0\varepsilon(\vec{r})\mu_0\frac{\partial^2\vec{H}(\vec{R},t)}{\partial t^2} = \nabla\times\vec{H}(\vec{r},t)\times(\nabla\ln\varepsilon_0\varepsilon(\vec{r})). \tag{2.20}$$

The modal fields can be expressed as

$$\vec{E} = \vec{e}(x,y)e^{i(\beta z-\omega t)} \tag{2.21}$$

$$\vec{H} = \vec{h}(x,y)e^{i(\beta z-\omega t)}, \tag{2.22}$$

where β is the propagation constant of the mode. The wave equations can then be written as

$$(\Delta_t + \omega^2 \varepsilon \varepsilon_0 \mu_0 - \beta^2)\vec{e_i} \tag{2.23}$$

$$(\Delta_t + \omega^2 \varepsilon \varepsilon_0 \mu_0 - \beta^2)\vec{h_i}, \tag{2.24}$$

with $i = x, y, z$ and the subscript t denotes the transversal component. These two equations yield two linear independent set of modes. If one sets $h_z = 0$, the solution is referred to as Transverse Magnetic Mode (TM). On the other hand, if one sets $e_z = 0$ the solution is called a Transverse Electric Mode (TE). With this, one arrives to the following equations

$$\frac{\partial^2 e_y(x)}{\partial x^2} + (\omega^2 \varepsilon \varepsilon_0 \mu_0 - \beta^2) e_y(x) = 0, \tag{2.25}$$

for the TE modes and

$$\frac{\partial^2 h_y(x)}{\partial x^2} + (\omega^2 \varepsilon \varepsilon_0 \mu_0 - \beta^2) h_y(x) = 0, \tag{2.26}$$

for the TM modes.

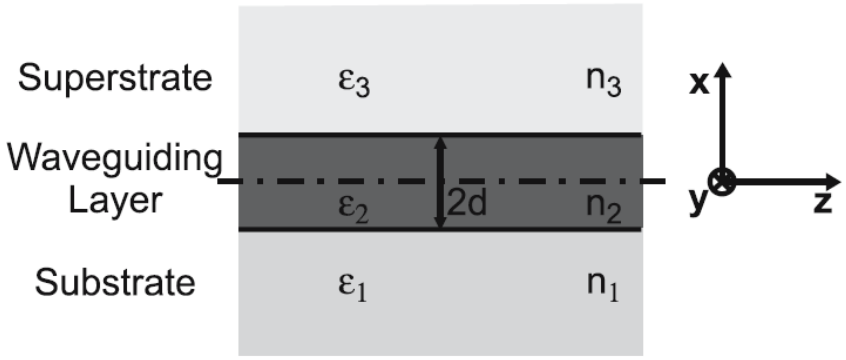

FIGURE 2.1: Section of a planar waveguide with a step refractive index profile.

Assuming that the section of the planar waveguide is of the form depicted in figure 2.1, one can transform the problem in two eigenvalue equations for TE and TM modes respectively as

$$\tan(kd) = \frac{\gamma_1/k + \gamma_3/k}{1 - (\gamma_1/k)(\gamma_3/K)} \tag{2.27}$$

$$\tan(kd) = \frac{\gamma_1 \varepsilon_2/k\varepsilon_1 + \gamma_3 \varepsilon_2/k\varepsilon_3}{1 - (\gamma_1 \varepsilon_2/k\varepsilon_1)(\gamma_3 \varepsilon_2/k\varepsilon_3)}, \tag{2.28}$$

where $k^2 = \omega^2 \varepsilon_2 \varepsilon_0 \mu_0 - \beta^2$ and $\gamma_{1,3} = \beta^2 - \omega^2 \varepsilon_{1,3} \varepsilon_0 \mu_0$.

With these equations, one can now assume that the waveguide is in fact a metal film sandwiched between two infinite dielectric media. If the metal thin film is much thicker than the penetration depth at each metal-dielectric interface, then the waveguide supports two TM modes, which correspond to a surface plasmon in each metal-dielectric interface. If the metal thickness decreases, the coupling between the two plasmons becomes increasingly stronger, which gives rise to mixed modes.

The modes of this dielectric-metal-dielectric waveguide can be found solving Eq. (2.28) using numerical methods.

2.2.2 Plasmons in a nano-wire

In this section, one will introduce the cylindrical Harmonics to analyse the plasmon polaritons of a metal nano-wire [39].

To describe the normal modes of a cylindrical structure, one should first introduce two dimensional scalar cylindrical harmonics, which are eigenfunctions of the Poisson equation

$$\nabla^2 V_m(k_z;\theta,z) = -\left(\frac{m^2}{r^2} + k_z^2\right) V_m(k_z;\theta,z), \tag{2.29}$$

where

$$V_m(k_z;\theta,z) = \frac{e^{i(m\theta+k_z z)}}{2\pi}, \tag{2.30}$$

with m as an integer and k_z represented as a real number.

Although these harmonics are scalar functions, one can perform a vector extension to obtain the orthogonal vector cylindrical harmonics

$$\vec{V}_m^r(k_z;\theta,z) = \vec{e}_r V_m(k_z;\theta,z), \tag{2.31}$$

$$\vec{V}_m^\theta(k_z;\theta,z) = \vec{e}_\theta V_m(k_z;\theta,z), \tag{2.32}$$

$$\vec{V}_m^z(k_z;\theta,z) = \vec{e}_z V_m(k_z;\theta,z). \tag{2.33}$$

where Eq. (2.31) is the radial vector, Eq. (2.32) is the tangential vector and Eq. (2.33) is the longitudinal vector.

With this in mind, an arbitrary vector field $\vec{G}(\theta,z)$ can be expanded as

$$\vec{G} = \sum_{m=-\infty}^{\infty} \int_{-\infty}^{\infty} dk_z \left[G_m^r(k_z)\vec{V}_m^r + G_m^\theta(k_z)\vec{V}_m^\theta + G_m^z(k_z)\vec{V}_m^z \right]. \tag{2.34}$$

In general, the normal modes in cylindrical geometry are hybrid, *i.e.* TM and TE polarizations are not independent from each other. However, one can still formally consider

the two polarizations separately because they will eventually couple through the boundary conditions.

For the TM polarization the electromagnetic field components are

$$H_m^z = 0, \tag{2.35}$$

$$H_m^r = \frac{m}{r}\frac{k_0\varepsilon}{k_0^2\varepsilon - k_z^2}E_m^z, \tag{2.36}$$

$$H_m^\theta = \frac{k_0\varepsilon}{k_0^2\varepsilon - k_z^2}\frac{dE_m^z}{dr}, \tag{2.37}$$

$$E_m^r = \frac{ik_z}{k_0^2\varepsilon - k_z^2}\frac{dE_m^z}{dr}, \tag{2.38}$$

$$E_m^\theta = -\frac{m}{r}\frac{k_z}{k_0^2\varepsilon - k_z^2}E_m^z, \tag{2.39}$$

where E_m^z has to obey

$$\frac{d^2E_m^z}{dr^2} + \frac{1}{r}\frac{dE_m^z}{dr} - \left(\frac{m^2}{r^2} - k_0^2\varepsilon + k_z^2\right)E_m^z = 0, \tag{2.40}$$

whereas for the TE polarizations the components are

$$E_m^z = 0, \tag{2.41}$$

$$E_m^r = -\frac{m}{r}\frac{k_0}{k_0^2\varepsilon - k_z^2}H_m^z, \tag{2.42}$$

$$E_m^\theta = -\frac{ik_0}{k_0^2\varepsilon - k_z^2}\frac{dH_m^z}{dr}, \tag{2.43}$$

$$H_m^r = \frac{ik_z}{k_0^2\varepsilon - k_z^2}\frac{dH_m^z}{dr}, \tag{2.44}$$

$$H_m^\theta = -\frac{m}{r}\frac{k_z}{k_0^2\varepsilon - k_z^2}H_m^z, \tag{2.45}$$

where H_m^z has to obey

$$\frac{d^2H_m^z}{dr^2} + \frac{1}{r}\frac{dH_m^z}{dr} - \left(\frac{m^2}{r^2} - k_0^2\varepsilon + k_z^2\right)H_m^z = 0. \tag{2.46}$$

The solution of Eqs. (2.40) and (2.46) are given by two different functions. For the region inside the metal, the solution of the equations are the cylindrical Bessel functions of the second kind ($j_m^{(2)}(k_\perp r)$). Whereas, for the region composed of the dielectric, the solution is given by the Hankel functions of the first kind ($h_m^{(1)}(k_\perp r)$).

Assuming a uniform infinite cylinder of radius R and $\varepsilon = \varepsilon_m$ embedded in a dielectric material with $\varepsilon = \varepsilon_d$, the TM and TE polarizations inside the cylinder, $r < R$, can be

written as

$$\left[E_m^z\right]_{metal} = d_m j_m(k_{metal\perp} r), \tag{2.47}$$

$$\left[H_m^z\right]_{metal} = -i\frac{k_{metal}}{k_0} c_m j_m(k_{metal\perp} r), \tag{2.48}$$

while in the surrounding medium, $r > R$, the two polarizations are given by

$$\left[E_m^z\right]_d = -a_m h_m(k_{d\perp} r), \tag{2.49}$$

$$\left[H_m^z\right]_d = i\frac{k_d}{k_0} b_m h_m(k_{d\perp} r), \tag{2.50}$$

where $k_{metal\perp} = \sqrt{k_0^2\varepsilon - k_z^2}$ and $k_{d\perp} = \sqrt{k_0^2\varepsilon - k_z^2}$ are the wavenumbers $k_\perp$ in the metal and in the dielectric media, respectively. The a_m, b_m, c_m and d_m are unknown constants that must satisfy the boundary conditions that imply the continuity of the tangential components of E_m^θ, E_m^z, H_m^θ, H_m^z on the cylinder boundary, $r = R$. With these conditions in mind, one can get the dispersion relations for the eigenfrequencies of the plasmon in this structure as a function of k_z

$$D_m^2(\omega, k_z) = W_m^{TM}(\omega, k_z) W_m^{TE}(\omega, k_z), \tag{2.51}$$

where

$$D_m(\omega, k_z) = m\frac{k_z}{k_0}\left(\frac{1}{k_{mt\perp}^2 R^2} - \frac{1}{k_{d\perp}^2 R^2}\right) j_m(k_{mt\perp} R) h_m(k_{d\perp} R), \tag{2.52}$$

$$W_m^{TM}(\omega, k_z) = \frac{\varepsilon_d}{k_{d\perp} R} j_m(k_{mt\perp} R) h_m'(k_{d\perp} R) - \frac{\varepsilon_{mt}}{k_{mt\perp} R} j_m'(k_{mt\perp} R) h_m(k_{d\perp} R), \tag{2.53}$$

$$W_m^{TE}(\omega, k_z) = \frac{1}{k_{d\perp} R} j_m(k_{mt\perp} R) h_m'(k_{d\perp} R) - \frac{1}{k_{mt\perp} R} j_m'(k_{mt\perp} R) h_m(k_{d\perp} R). \tag{2.54}$$

Solving these equations, one can obtain the complex wavenumber k_z of the modes, which, as it was already mentioned, are hybrid. One can see in figure 2.2 the dependence of the complex wavenumber on energy.

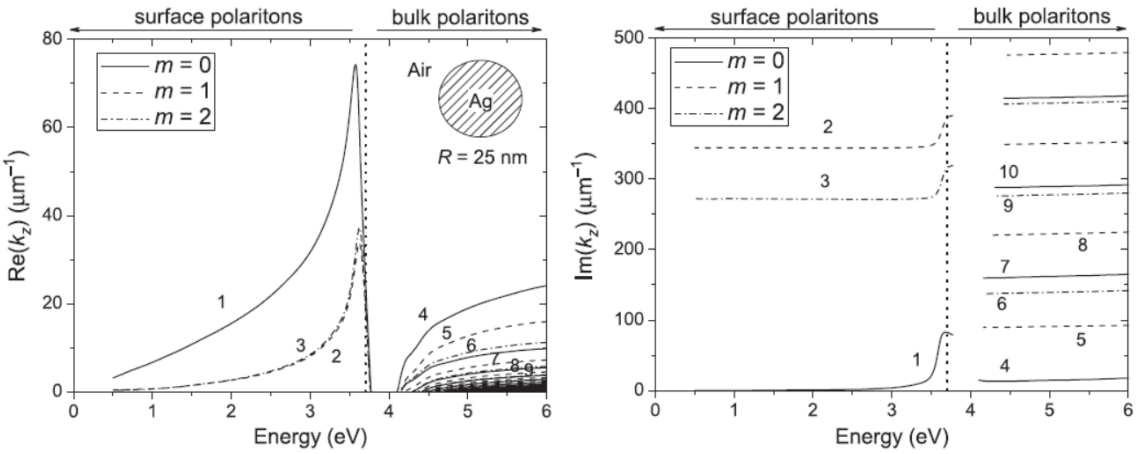

FIGURE 2.2: The dependence of the complex wavenumber k_z on the energy for plasmon polaritons with azimuthal numbers ($m = 0, 1, 2$) propagating in a silver nanowire of radius $R = 25$ nm. The vertical dotted line shows the level of the plasma energy, $\hbar\omega_p$ [2]

.

2.2.3 Plasmons in nano-spheres

The vector spherical-harmonics formalism will be, firstly, introduced in this section and then used to study the plasmonic modes of a sphere [39].

Scalar spherical harmonics $Y_{l,m}(\theta, \phi)$ are two-dimensional eigenfunctions of the Poisson equation [2]

$$\nabla^2 Y_{l,m}(\theta, \phi) = -\frac{l(l+1)}{r^2} Y_{l,m}(\theta, \phi), \tag{2.55}$$

where

$$Y_{l,m}(\theta, \phi) = N e^{im\phi} P_{l,m}(\theta, \phi) \tag{2.56}$$

and $P_{l,m}(\theta, \phi)$ are the Legendre polynomials.

Since the electromagnetic field is a vector field, a vector extension is needed to represent the electromagnetic field with the spherical harmonics. There are numerous ways to perform this extension, one of which is

$$\vec{Y}^{(1)}_{l,m} = \frac{\vec{r}}{r} Y_{l,m}(\theta, \phi) \tag{2.57}$$

$$\vec{Y}^{(2)}_{l,m} = \frac{r \nabla Y_{l,m}(\theta, \phi)}{\sqrt[2]{l(l+1)}} \tag{2.58}$$

$$\vec{Y}^{(3)}_{l,m} = \frac{\vec{r} \times \nabla Y_{l,m}(\theta, \phi)}{\sqrt[2]{l(l+1)}}, \tag{2.59}$$

where Eq. (2.57) defines the radial vector, while Eqs. (2.58) and (2.59) the two tangential vectors of the sphere surface.

With these three vectors, it is possible to write a given vector field G as

$$\vec{G} = \sum_{l=0}^{\infty} \sum_{m=-l}^{l} [G_{l,m}^{(1)} \mathrm{Y}_{l,m}^{(1)} + Gl, m^{(2)} \mathrm{Y}_{l,m}^{(2)} + Gl, m^{(3)} \mathrm{Y}_{l,m}^{(3)}]. \tag{2.60}$$

Then, the Curl of G is given by

$$\begin{aligned} \nabla \times \vec{G} = \sum_{l=0}^{\infty} \sum_{m=-l}^{l} \Bigg[& -\frac{l(l+1)}{r} G_{l,m}^{(3)} \mathrm{Y}_{l,m}^{(1)} - \left(\frac{dGl, m^{(3)}}{dr} + \frac{Gl, m^{(3)}}{r} \right) \mathrm{Y}_{l,m}^{(2)} + \\ & \left(-\frac{Gl, m^{(1)}}{r} + \frac{dGl, m^{(2)}}{dr} + \frac{Gl, m^{(2)}}{r} \right) \mathrm{Y}_{l,m}^{(3)} \Bigg]. \end{aligned} \tag{2.61}$$

If Eqs. (2.57), (2.58), (2.59) and (2.61) are applied to the electromagnetic field, the Maxwell equations split in two independent modes, the Transverse Magnetic (TM) and the Transverse Electric (TE) modes.

The TM modes have two non-zero electric components,

$$E_{l,m}^{(1)} = -\frac{i}{k_0 \varepsilon} \frac{l(l+1)}{r} H_{l,m}^{(3)} \tag{2.62}$$

$$E_{l,m}^{(2)} = -\frac{i}{k_0 \varepsilon} \frac{dH_{l,m}^{(3)}}{dr} + \frac{H_{l,m}^{(3)}}{r}, \tag{2.63}$$

where $H_{l,m}^{(3)}$ has to obey

$$\frac{d^2 H_{l,m}^{(3)}}{dr^2} + \frac{2}{r} \frac{dH_{l,m}^{(3)}}{dr} - \left[\frac{l(l+1)}{r^2} - k_0^2 \varepsilon \right] H_{l,m}^{(3)} = 0. \tag{2.64}$$

Whereas the TE mode features two non-zero magnetic field components

$$H_{l,m}^{(1)} = \frac{i}{k_0} \frac{l(l+1)}{r} E_{l,m}^{(3)}, \tag{2.65}$$

$$E_{l,m}^{(2)} = -\frac{i}{k_0} \frac{dE_{l,m}^{(3)}}{dr} + \frac{E_{l,m}^{(3)}}{r} \tag{2.66}$$

and $E_{l,m}^{(3)}$ follows

$$\frac{d^2 E_{l,m}^{(3)}}{dr^2} + \frac{2}{r} \frac{dE_{l,m}^{(3)}}{dr} - \left[\frac{l(l+1)}{r^2} - k_0^2 \varepsilon \right] E_{l,m}^{(3)} = 0. \tag{2.67}$$

The solution of Eqs. (2.40) and (2.46) are given by two different functions. For the region inside the metal, the solution of the equations are the spherical Bessel functions of the second kind ($j_m^{(2)}(k_\perp r)$). On the other hand, for the region composed of the dielectric, the solution is given by the Hankel functions of the first kind ($h_m^{(1)}(k_\perp r)$).

Applying this to a uniform metal sphere of radius (R) with $\varepsilon = \varepsilon_m$ embedded in a dielectric material with $\varepsilon = \varepsilon_d$, the fields for the TM and TE modes when $r \leq R$ can be written as

$$\left[H^{(3)}_{l,m}\right]_m = -i\frac{k_m}{k_0} d_{lm} j^{(2)}_l(k_m r) \tag{2.68}$$

$$\left[E^{(3)}_{l,m}\right]_m = c_{lm} j^{(2)}_l(k_m r), \tag{2.69}$$

and when $r > R$:

$$\left[H^{(3)}_{l,m}\right]_d = i\frac{k_d}{k_0} a_{lm} h^{(1)}_l(k_e r) \tag{2.70}$$

$$\left[E^{(3)}_{l,m}\right]_d = -b_{lm} h^{(1)}_l(k_d r), \tag{2.71}$$

where a_{lm}, b_{lm}, c_{lm} and d_{lm} are constants that can be determined by the boundary conditions. The dispersion relations for the eigenfrequencies of the plasmon in this structure is

$$q_m \psi_l(q_m)\eta'_l(q_m) - q_d \eta_l(q_d)\psi'_l(q_m) = 0, \tag{2.72}$$

for the TM mode. While for the TE they are given by

$$q_d \psi_l(q_m)\eta'_l(q_d) - q_m \eta_l(q_m)\psi'_l(q_m) = 0, \tag{2.73}$$

where $\psi_l(q_m) = q_m j_l(q_m)$ and $\eta_l(q_d) = q_d h_l(q_m)$ are the Riccati-Bessel functions, being $q_m = K_m R$ and $q_d = K_d R$.

Solving these equations, one can obtain the eigenfrequencies of the normal modes. These frequencies are complex, where the real part determines the plasmon energy ($E_l = \omega_r \hbar$) and the imaginary part characterizes the lifetime of the plasmon ($t_l = -1/(2\omega_i)$. The bulk plasmons exist at $E > \hbar\omega_p$ and the surface plasmons exist at $E < \hbar\omega_p$. Even though there can be solutions for TE modes for surface plasmons, commonly they have little to no relevancy, since their lifetime are quite small compared to the TM modes ($Im(w_l) << 0$).

As one can see in figure 2.3 the plasmonic modes, in particular those comprised of surface plasmons, could be compared with the discrete energy levels of an electron in an atom. This analogy will be even more unequivocal if one uses the semi-classical model stated in the next section.

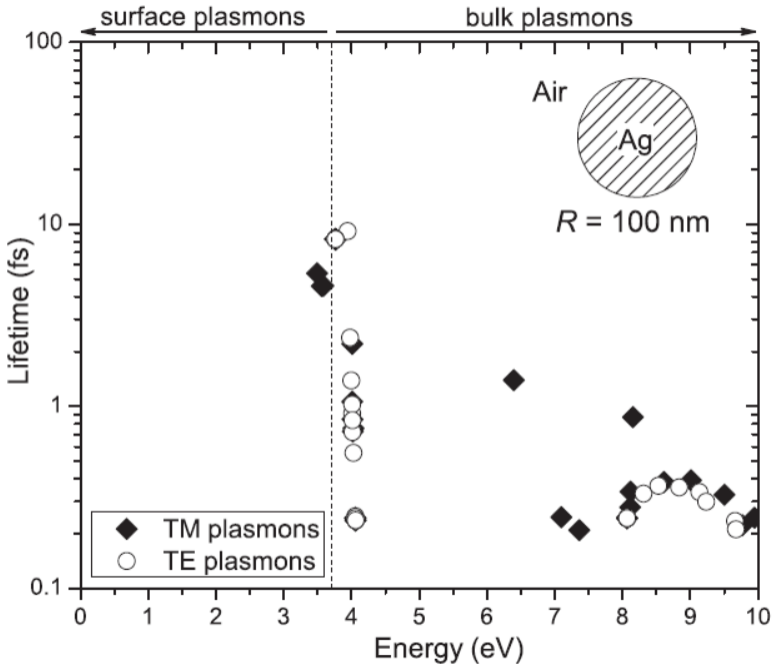

FIGURE 2.3: Surface and Bulk Plasmons of a spherical nano-particle with R=100nm. The dashed line shows the plasma energy $\hbar\omega_p$ [2].

2.3 The Semi-Classical Model for Plasmons

Up until now, the focus of this work has been the description of the classical treatment for plasmons. However, for nanostructures the behaviour of plasmons starts to gain quantum features and it is necessary to develop a semi-classic model using the fluid equations for the conduction electrons that compose plasmons in metals. The solutions of the fluid equations can be obtained using an analogue quantum mechanical problem under the Madelung formalism, namely by solving a Nonlinear Schrödinger Equation, for example using numerical methods.

Recently, *Ciracì et al.* have applied the hydrodynamic description of electrons in numerical simulations of plasmonic nanostructures and obtained predictions that are in agreement with the experimental data [19]. Although this model provides a description of some quantum phenomena, such as the electron-electron Coulomb interaction and the Pauli Exclusion Principle, it still fails to account for the tunnelling effect and the quantum oscillations, for example.

The motion of electrons in a metal under the influence of an electromagnetic field can be described according to the hydrodynamical model by the fluid equations [40]

$$-\partial_t n = \nabla \cdot (n\vec{u}) \tag{2.74}$$

$$n\partial_t \vec{u} + n(\vec{u}\cdot\nabla)\vec{u} = -\frac{ne}{m_e}(\vec{E} + \vec{u}\times\vec{B}) - \frac{\nabla P}{m_e} - \gamma n\vec{u}, \tag{2.75}$$

where n, $\vec{u}$, m and q are the electron density, velocity mass and charge, respectively, and $\vec{E}$ and $\vec{B}$ are the electric and magnetic fields of the electromagnetic radiation. The terms in the right side of Eq. (2.75) represent the Lorentz force, the Thomas-Fermi pressure (a pressure that accounts for the Pauli Exclusion Principle, with $P = (3\pi^2)^{2/3}\frac{\hbar^2}{5m}n^{5/3}$) and the damping forces (a phenomenological parameter that accounts for the damping due to electron-ion collisions), respectively [19]. With these two equations one can now apply the Madelung Formalism to re-express Eq. (2.74) and Eq. (2.75) as a Non-linear Schrödinger equation. The application of the Madelung Formalism is a rather cumbersome process and, for that reason, the details are presented in appendix A.

The Madelung Formalism was initially established to re-express the Schrödinger equation in terms of fluid equations that describe the flow of probability of the wave-function in quantum systems. In this particular case, one applies it in the opposite way. By that, one defines the plasmons in a metal by describing electrons by a wave-function [41],

$$i\hbar\partial_t\psi = \Big(-\frac{\hbar^2}{2m}\nabla^2 + V_{eff}\Big)\psi, \tag{2.76}$$

where $n = n_0\psi^*\psi$, n_0 is the mean electron density, $\vec{u} = \frac{\hbar}{m}\nabla\mathcal{S}$ and $\mathcal{S} = arg(\psi)$. However, one should be careful in using this formalism as the potential in the Schrödinger equation, V_{NonL}, is a non-linear potential defined by

$$V_{eff} = V_c + V_L + V_{NL}, \tag{2.77}$$

where V_c is the potential that takes into account the geometry of the plasmonic system, V_L is the Lorentz potential from the applied electromagnetic field and where V_{NL} is given by

$$V_{NL} = \frac{\hbar^2}{2m}\frac{\nabla^2\sqrt{n}}{\sqrt{n}} + \alpha n^{\frac{5}{3}}, \tag{2.78}$$

where the first term is the Bohm potential and the second the Thomas-Fermi pressure, with $\alpha = \frac{(3\pi^2)^{\frac{2}{3}}}{5m}\hbar$.

Due to the complexity of this equation, the solutions of Eq. 2.76 were divided in two:

the linear solutions and, after, the solution including the non-linear potentials. This organisation was sought because, if one considers only the linear terms, the analogy between plasmons and an electron in an atom can be established.

2.4 Conclusions

This chapter reviews the models used to describe plasmons and establishes an analogy between plasmonic systems and quantum mechanics. This analogy suggests that the plasmonic modes in a nano-scale structure can be mapped into the energy levels of an electron trapped in a potential well. However, one can take this analogy further and investigate whether the physical phenomena associated with atoms or electrons in potential wells could have a plasmonic counterpart, and more importantly, if those phenomena could be used as sensing principles. Indeed, there have been many studies in the literature where metallic quantum dots exhibit effects that one is accustomed to associate with atoms, such as resonant absorption and emission, luminescence or shifts in optical response due to local electromagnetic fields.

The analogy between plasmons confined in nano-scale structures and atomic systems is not entirely new. But what is new is the formal bridge established between the hydrodynamical Drude model and the Schrödinger equation. Localized plasmons will have characteristic properties that can be customized by choosing the shape, size and material of the nano-structure. Combining such structures would allow to have plasmonic chemistry, just like combining atoms would lead to molecules. As Richard Feynman said "There is plenty of room at the bottom" [1], and that could be nano-plasmonics.

The connection between the two models introduces another ingredient not present in the quantum model for atoms which is the non-linearity. Quantum mechanics is a linear theory which as a critically a consequence of the superposition principle. If the non-linear effects are too strong, they may affect and even break the analogy between plasmonics and quantum mechanics. As a result this approach would end here. Furthermore solving non-linear quantum problems is a troublesome challenge where standard analytical and numerical solvers fail.

Having all this in mind, the following chapters will investigate how damaging can the non-linear effects be to the analogy between the hydrodynamic Drude model for plasmonics and the quantum model for a single electron.

[1] Richard Feynman in American Physical Society meeting at Caltech on December 29, 1959.

Chapter 3

The Linearised Schrödinger Equation

The previous chapter established an analogy between the hydrodynamic Drude model for plasmons and the the quantum model for a single electron trapped in a non-linear potential. Unfortunately, it is extremely difficult to find the solutions for the non-linear quantum equations and most of the insight of linear quantum mechanics may fail if the non-linearities are strong enough.

However, as a first step, it is important to consider a linear approximation of Eq. 2.76. A simple method to achieve this is to neglet the non-linear terms and reduce Eq. 2.76 to

$$i\hbar\partial_t\psi = \Big(-\frac{\hbar^2}{2m}\nabla^2 + V_{Lin}\Big)\psi, \tag{3.1}$$

where V_{Lin} is the potential defined by

$$V_{Lin} = V_c + V_L, \tag{3.2}$$

with V_c as the potential that takes into account the geometry of the plasmonic system and V_L the Lorentz potential from the applied electromagnetic field.

For bulk plasmons or plasmons in large scale structures, the solutions of Eq. 3.1 are very easy to obtain using approximations such as the Wentzel-Kramers-Brillouin method, and are basically plane waves without important features.

However, when one considers plasmons confined in structures of a few nanometres, i. e. the typical scale of an atom (or a few atoms) things change dramatically.

At these scales the Eq. 3.1 describes plasmons that are analogue to strongly confined electrons in a potential. Then, the solutions of Eq. 3.1 include trapped states separated by large band gaps, just like electrons in an atom.

This establishes an analogy between plasmons and an electron in an atom and justifies why a collective phenomenum (involving in excess of 10^{30} electron) mimics the behaviour of a quantum system. For example, if one considers two touching nano-wires embedded in the core of a fibre optics, the cross section of said system could be understood as an analogy to a diatomic molecule. But this analogy can be taken further. These artificial atoms and molecules exhibit the same type of effects of real atoms and molecules, as they can be Stark shifted by an external electric field, probed by electromagnetic waves, with potential applications in sensing, a topic that will be explored further in this dissertation project.

The static solutions can be given by the following equation

$$\varepsilon\psi = \Big(-\frac{\hbar^2}{2m}\nabla^2 + V_{Lin}\Big)\psi. \tag{3.3}$$

The energy level of the resulting molecular plasmonic modes can be further modified by the presence of a static external electric field $\vec{E}_{stat}$, which produces a DC Stark effect. The energy levels resulting from the coupling between the wires and the action of $\vec{E}_{stat}$ can be computed by solving Eq. 3.3 with

$$V_L = e\vec{r} \times \vec{E}. \tag{3.4}$$

If instead the dimer is affected by an oscillating field and this field is tuned to the energy difference between two different plasmonic modes, it is possible to excite Rabi oscillations between them. This will promote a high absorbance in the wavelength characterized by the energy difference of the states which form the Rabi oscillations.

3.1 Numerical Method for the Stationary Linear Schrödinger Equation

Eq 3.3 falls into a category of eigenproblems for the which there is a wide range of numerical problems. Among them, the Finite Difference method recasts the problem as an algebraic eigenproblem by replacing the Laplacian with the adequate finite difference.

For example in a two dimensional system, the wave function can be represented by its values over a square grid with finite size, as represented in Figure 3.1.

Then, the Laplacian at the grid point with horizontal and vertical indexes i and j, respectively, is given by

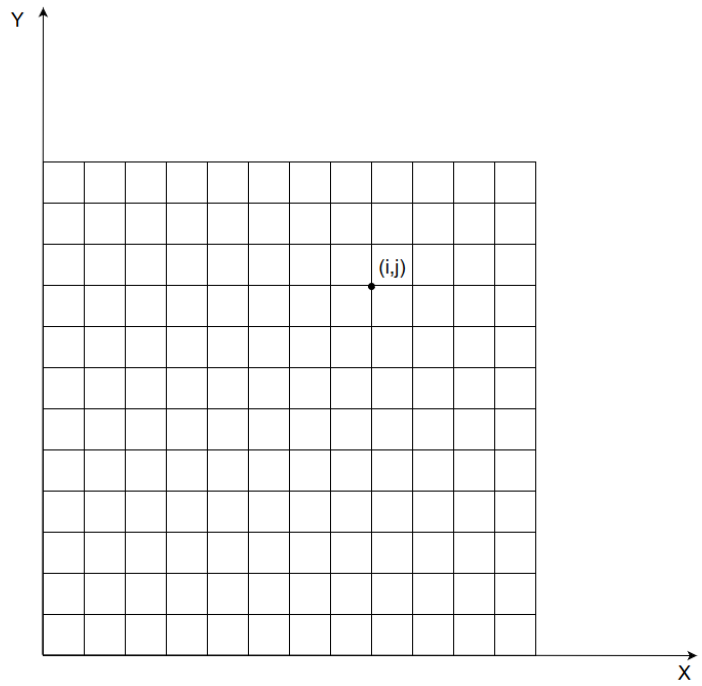

FIGURE 3.1: Representation of a square grid where the wave-function is expressed.

$$\Delta\psi_{i,j} \approx \frac{\psi_{i+1,j} + \psi_{i-1,j} + \psi_{i,j+1} + \psi_{i,j-1} - 4\psi_{i,j}}{\hbar^2}. \tag{3.5}$$

Combining the finite differences for all the points in the sampling grid, Eq. 3.5 can be casted in matrix form, such that

$$\nabla \begin{pmatrix} \psi_{0,0} \\ \psi_{0,1} \\ \psi_{0,2} \\ \dots \\ \psi_{N,N} \end{pmatrix} = \mathbf{M} \begin{pmatrix} \psi_{0,0} \\ \psi_{0,1} \\ \psi_{0,2} \\ \dots \\ \psi_{N,N} \end{pmatrix} \tag{3.6}$$

As a result, a numerical approximation of Eq. 3.3 can be written

$$\varepsilon x = \mathbf{A} x \tag{3.7}$$

with $x = \begin{pmatrix} \psi_{0,0} \\ \dots \\ \psi_{N,N} \end{pmatrix}$, $A_{i,j} = -\frac{\hbar^2}{2m} M_{i,j} + V_{Lin,i,j}$ and $V_{Lin,i,j} = V_{Lin}(r_i, j)$. This corresponds to a simple algebraic eigenproblem equation and can be solved numerically using sparse matrices, as provided by *Python* module *scipy.sparse*.

3.2 Computational Results for the Linear Solutions

This section shows the results from the implementation in *Python* of the linear solutions of the system. The first step was to verify the effect of the electrostatic field in the eigenstates.

Figures 3.2 and 3.3 show the eigenstates of a system composed by two overlapping nano-wires. As one can see, the results establish an analogy between the plasmonic modes and an electron trapped in a potential well. These results also show that an applied static electric field can dramatically alter the electron density distribution of the plasmon modes depending on the amplitude and propagation state of the field, which leads to a change of the optical response, and in particular in the absorption spectrum.

In these figures, the electron densities are represented by the color scales and the single line represents the confining potential.

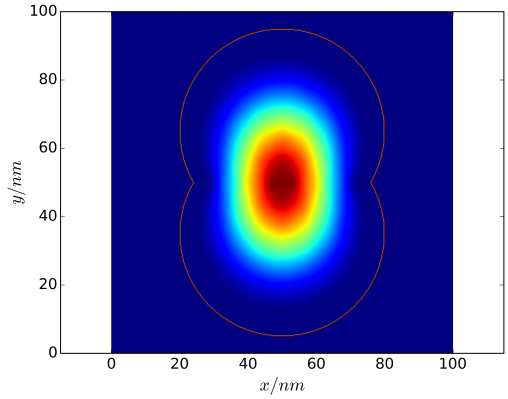

(A) The electron density distribution for the first plasmonic energy level with $\vec{E}_{static} = 0$ and $\theta = 0$

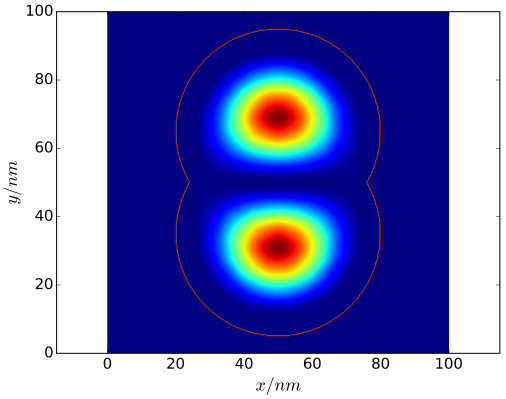

(B) The electron density distribution for the second plasmonic energy level with $\vec{E}_{static} = 0$ and $\theta = 0$

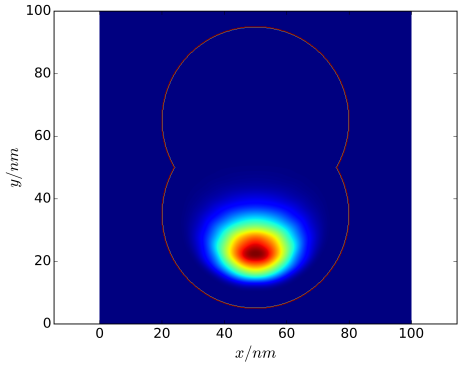

(C) The electron density distribution for the first plasmonic energy level with $\vec{E}_{static} = 10$ and $\theta = 0$

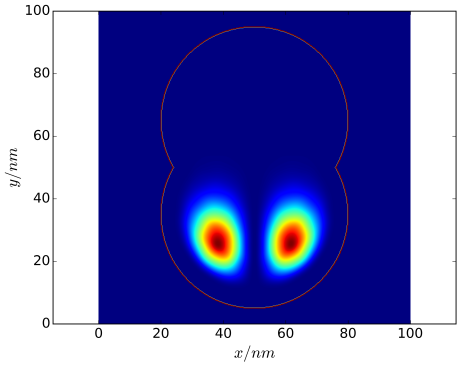

(D) The electron density distribution for the Second plasmonic energy level with $\vec{E}_{static} = 10$ and $\theta = 0$

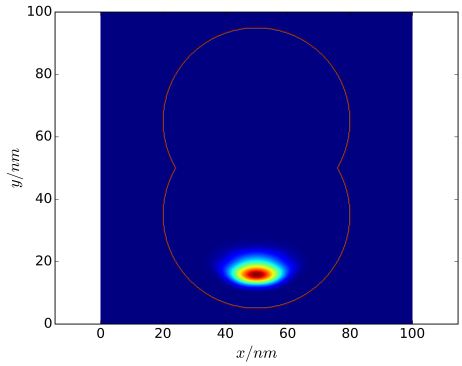

(E) The electron density distribution for the first plasmonic energy level with $\vec{E}_{static} = 10^2$ and $\theta = 0$

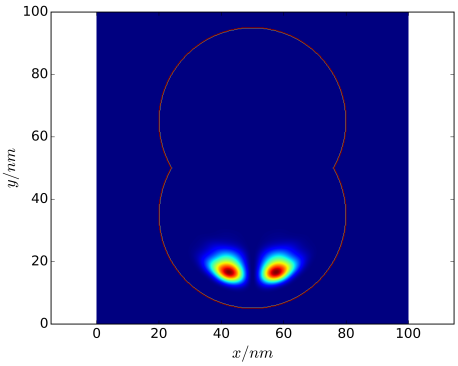

(F) The electron density distribution for the second plasmonic energy level with $\vec{E}_{static} = 10^2$ and $\theta = 0$

FIGURE 3.2: The electron density distribution for different $\vec{E}_{stat}$ with $\theta = 0$

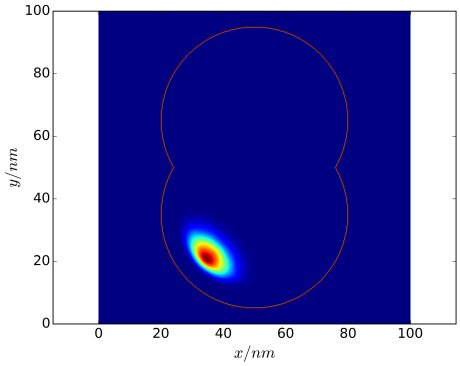

(A) The electron density distribution for the first plasmonic energy level with $\vec{E}_{static} = 10^2$ and $\theta = \frac{\pi}{6}$

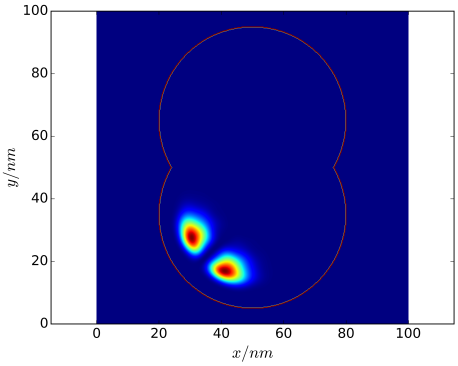

(B) The electron density distribution for the second plasmonic energy level with $\vec{E}_{static} = 10^2$ and $\theta = \frac{\pi}{6}$

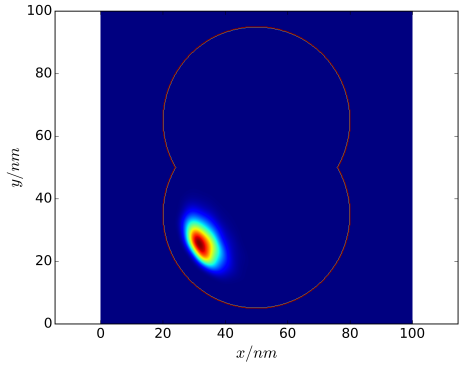

(C) The electron density distribution for the first plasmonic energy level with $\vec{E}_{static} = 10^2$ and $\theta = \frac{\pi}{4}$

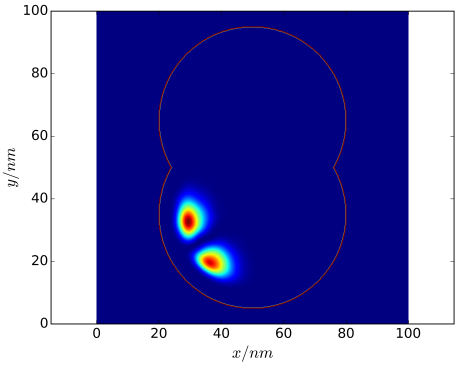

(D) The electron density distribution for the second plasmonic energy level with $\vec{E}_{static} = 10^2$ and $\theta = \frac{\pi}{4}$

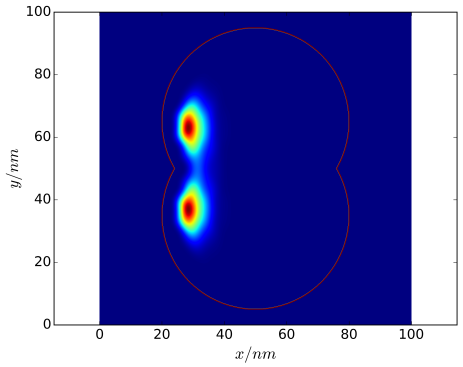

(E) The electron density distribution for the first plasmonic energy level with $\vec{E}_{static} = 10^2$ and $\theta = \frac{\pi}{2}$

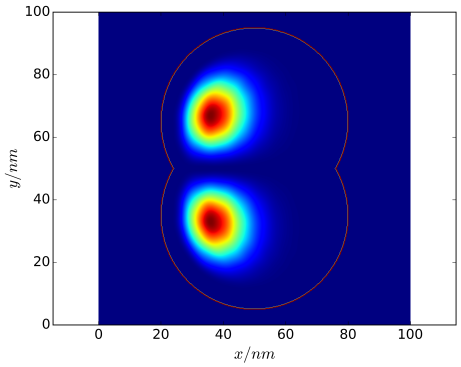

(F) The electron density distribution for the second plasmonic energy level with $\vec{E}_{static} = 10^2$ and $\theta = \frac{\pi}{2}$

FIGURE 3.3: The electron density distribution for different $\vec{E}_{stat}$ with $\theta = \frac{\pi}{2}$

It was also considered the case where the nano-wires have a square cross-section as opposing to circumferences, as represented in Fig 3.4. In order to optimize the sensor one started to study the variation of the distance D while also increasing the static electric field.

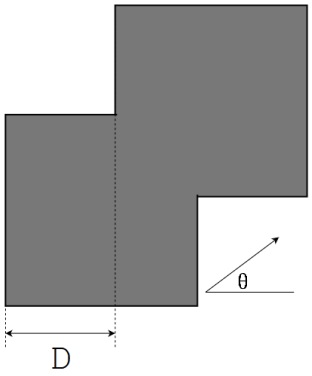

FIGURE 3.4: Geometry of an overlapping square dimer with plasmonic modes similar to those of a chemical bond in diatomic molecules. The strength of the analogous chemical bond is proportional to the overlap.

Figure 3.5 presents some eigenstates obtained. In particular, Figure 3.5a shows the first energy level with $\vec{E} = \vec{0}$ and $D = 10.1nm$. This model is only valid for overlapping monomers since if closely separated the tunnelling of electrons between them is promoted, an effect not included in our approach [23]. Figure 3.5b shows the first eigenstates with $\vec{E} = \vec{0}$ and $D = 2.0nm$. In figures 3.5c and 3.5d the first and second energy levels, respectively. One should notice the clear distinction between these two eigenstates as the first is the symmetric solution whereas the other one is the anti-symmetric.

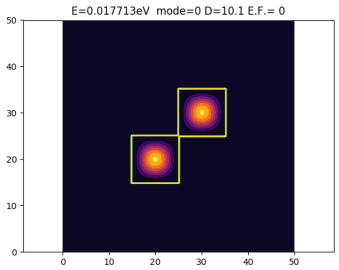

(A) $|\vec{E}| = 0, D = 10.1, Mode = 0$

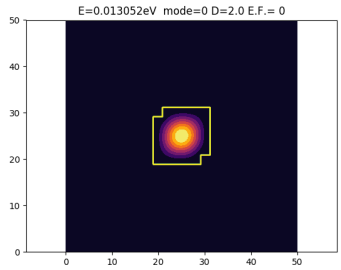

(B) $|\vec{E}| = 0, D = 2.0, Mode = 0$

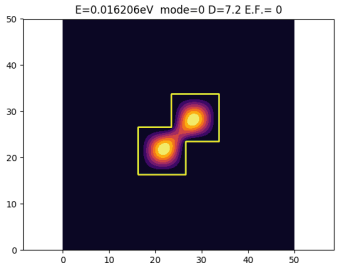

(C) $|\vec{E}| = 0, D = 7.2, Mode = 0$

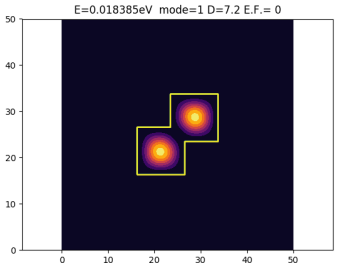

(D) $|\vec{E}| = 0, D = 7.2, Mode = 1$

FIGURE 3.5: Electron density distribution for different D in nanometres. The lines indicate the limits of the dimers.

With these results in mind one can now try to solve the non-linear Schrödinger equation and compare. This is done in the next chapter, where first the numerical method is presented and tested, then the results are shown and finally compared to the ones obtained here.

3.3 Conclusions

This chapter investigated the solutions of the linearised Schrödinger equation used as an analogue of the original hydrodynamic model for plasmons. By removing the non-linear potentials we have neglected the quantum effects produced by the Thomas-Fermi potential, and associated with the exclusion principle. This process allows to apply the techniques developed for quantum mechanics and provides a one-to-one analogue between the plasmon and the electron trapped in a potential. However, one needs to question the validity of not considering the non-linear terms in the Schrödinger equation. This will be addressed in the next chapter.

Chapter 4

Schrödinger Equation: Non-Linear Solutions

As shown in chapter 2, the Madelung formalism implies that the solutions of the non-linear Schrödinger equation can be mapped into solutions of the hydrodynamic Drude model for plasmons. However, solving this equation is not an easy task, and therefore the previous chapter investigated the properties of linear approximation of this equation. For small non-linearities, it is possible to improve these linear approximation using perturbation theory however, this is not the case. The energy associated with the Thomas-Fermi potential is larger by several orders of magnitude than the kinetic energy of a trapped electron and therefore there is no guarantee that the perturbative approach is adequate. So another method to verify how much the linear solutions are altered when the non-linear term is introduced in Eq. 2.76 is needed.

To investigate this, one adopts another strategy and analyses how much the ground state of the plasmonic atom or molecule is affected by the inclusion of the non-linear terms. This presents an advantage since the ground state can be calculated by energy minimization methods. Basically one searches for solutions of the non-linear eigenproblem

$$\varepsilon\psi = \left(-\frac{\hbar^2}{2m}\nabla^2 + V_L + V_{NL}\right)\psi, \tag{4.1}$$

which minimize the energy ε. Then, comparing the properties of this non-linear solution with its linear approximation allows to extrapolate for other states and ultimately tests how good this approximation is.

4.1 Numerical Method for the Non-Linear Solutions

With the insight provided by the linear solutions, one can now solve Eq. 2.76 with the non-linear terms. In this equation, the Hamiltonian takes the form

$$H = H_0 + F, \tag{4.2}$$

where $H_0 = -\frac{\hbar^2}{2m}\nabla^2 + V_L$ is the linear Hamiltonian and $F = (3\pi^2)^{\frac{2}{3}}\hbar n^{\frac{5}{3}}/5m$ is the Thomas-Fermi potential.

Comparing Eq. 4.2 with Eq. 2.76, one notices that they are not exactly the same since F does not include the Bohn potential, which also is a non-linear term just like the Thomas-Fermi potential. This can be justified since the Bohn potential is small enough to be considered negligible.

The expected value of this Hamiltonian can be described as a function of the wave-function

$$\mathcal{H}(\psi) = \langle\psi| H |\psi\rangle = \int dr^n \psi^*(r) H\psi(r). \tag{4.3}$$

It is also convenient to define

$$\mathcal{F}(\psi) = \int dr^n \psi^*(r) \mathcal{F}\psi(r) \tag{4.4}$$

$$\mathcal{H}_0(\psi) = \int dr^n \psi^*(r) \mathcal{H}_0\psi(r). \tag{4.5}$$

Since both $\mathcal{H}_0$ and $\mathcal{F}$ are positive functions, it follows that the function $\mathcal{H}(\psi)$ must have a minimum, which corresponds to the ground state satisfying

$$\delta_\psi \mathcal{H}(\psi) = 0, \tag{4.6}$$

where δ_ψ is the functional derivative.

This property can be used to devise a numerical method of finding the ground state. One now considers the numerical approximation of the functions 4.4 and 4.5.

$$\mathcal{F}(x) = \sum \psi^*_{i,j} \mathcal{F}_{i,j} \psi_{i,j} \tag{4.7}$$

$$\mathcal{H}_0(x) = \sum \psi^*_{i,j} \mathcal{H}_0 i, j \psi_{i,j}, \tag{4.8}$$

where x is a vector containing the values of $\psi_{i,j}$ for all sampling points on a grid. Then, the condition 4.6 becomes

$$\delta_x \mathcal{H}(x) = 0, \tag{4.9}$$

which leads to

$$\partial_x \mathcal{H}_0(x) = -\partial_x \mathcal{F}(x). \tag{4.10}$$

The numerical method used in chapter 3 to solve the linear eigenproblem is very intuitive. In contrast the implementation of Eq. 4.10 is not as straightforward because the eigenproblem is non-linear. Instead, one develops a numerical equation based on Eq. 4.10 by defining the operators $\mathbf{A}$ and $\mathbf{B}$, such that $\mathbf{A}x = \partial_x \mathcal{H}_0(x)$ and $\mathbf{B}x = \partial_x \mathcal{F}(x)$. This means that equation 4.10 simplifies to

$$\mathbf{A}x = -\mathbf{B}x. \tag{4.11}$$

The operator $\mathbf{A}$ has to be inverted for this equation to be implemented but this might not be well conditioned numerically. Instead one writes Eq. 4.10 in an equivalent form.

$$(\mathbf{1} - \xi\mathbf{A})x = (\mathbf{1} + \xi\mathbf{B})x \tag{4.12}$$

where $\mathbf{1}$ is the unity matrix, ξ a small number choosen to guarantee convergence, *i. e.*, for small values of ξ the calculations of the inverse of $\mathbf{1} - \xi\mathbf{A}$ are always well conditioned.

Eq. 4.12 can then be transformed into

$$x = (1 - \xi\mathbf{A})^{-1}(1 - \xi\mathbf{B})x. \tag{4.13}$$

For small values of ξ leads to

$$(1 - \xi\mathbf{A})^{-1} \approx \mathbf{1} + \xi\mathbf{A}. \tag{4.14}$$

With this one can create an iterative method

$$x^{n+1} = (\mathbf{1} + \xi\mathbf{A})\mathbf{B}x^n, \tag{4.15}$$

where x^0 is the initial guess.

As previously said, the numerical method used is not standard, so to test it one started by doing a 1-dimensional implementation. In this case one considers the potential

$$V_c = \begin{cases} 1 - \exp\left(-\left(\frac{x-\frac{d}{2}}{R}\right)^{20}\right) & \text{for the left well} \\ 1 - \exp\left(-\left(\frac{x+\frac{d}{2}}{R}\right)^{20}\right) & \text{for the right well,} \end{cases} \tag{4.16}$$

where R is the length of the well, which in this case was considered $10nm$.

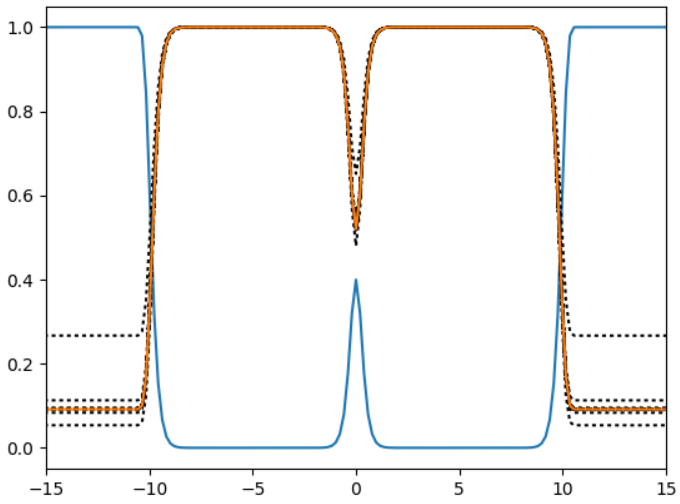

FIGURE 4.1: Numerical method test for two wells separated by $d = 10nm$. The confining potential is shown in blue, the solution in orange and the dashed lines represent evolution of the approximate solution after 100 iterations.

This describes two potential wells in one dimension with smooth edges described by two Gaussian distributions, one for each potential. This will be the seed solution to be used in the numerical method. After several iterations, the solutions can be found in Figure 4.1. This solution is very close to what is expected as the electron density is spreaded evenly over the potential well as a result of the electron repulsion due to the Pauli exclusion principle.

4.2 Computational Results for the Non-Linear Solutions

To compare the linear and the non-linear solutions it was considered the case with two nano-wire with square cross section, previously investigated in chapter 3. The idea is to analyse the changes introduced by the non-linear potentials in the dependency of the

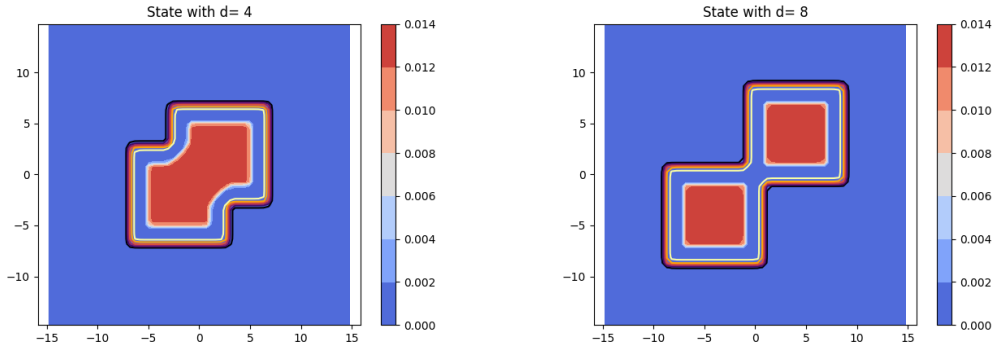

(A) The electron density distribution with $D = 2nm$.

(B) The electron density distribution with $D = 6nm$.

FIGURE 4.1: The electron density distribution for different values of D

ground state of the analogue electron as a function of the overlap between the wires, expressed in term of the distance D.

The inclusion of the non-linear potential will produce an increase of energy of the ground state due to the inclusion of an extra term in the Hamiltonian in Eq. 3.1. However, the absolute value of the energy has little meaning instead, what is important is the change in the band gap between two consecutive states, which will correspond to the photon frequencies that can be absorbed by the plasmons. Therefore, to compare the results from the linear and non-linear model, one needs to consider the change in energy of the ground state for different values of D with and without the non-linear term. To do this, one adopts a reference configuration corresponding to the total overlap between the two wires (occurring when $D = 0$) and compute the value of

$$\Delta E = E_{D=0} - E_{D=d}, \tag{4.17}$$

where $E_{D=0}$ is the energy level where the squares are completely overlapped and $E_{D=d}$ is the energy level where the distance between the squares is d. The difference in values ΔE for two consecutive sates is identical to the band gaps of the plasmonic modes and therefore, can be used to analyse the results just as well.

Although the numerical method for the non-linear problem converges towards a minimum of energy, it is a very slow algorithm and each simulation can take up to a day. In the first iterations, the main changes to the electron distribution occur near the edges of the wires while the electron density in the interior of the wires remains practically flat. Only after several iterations it is possible to observe changes of the electron density in the

interior of the wires but which are very small. The final electron distribution are illustrated in Figure 4.1 and they are basically an extension of the 1-dimensional case previously described. The electron density remains flat in the interior of the wires as a result of the electron repulsion due to the Pauli exclusion principle, which prevents two or more electrons to occupy the same state and, in this case, the same position. This forces the electrons to spread out as evenly as possible through the interior of the wires. The only exception to this occurs near the edges where boundary effects are predominant.

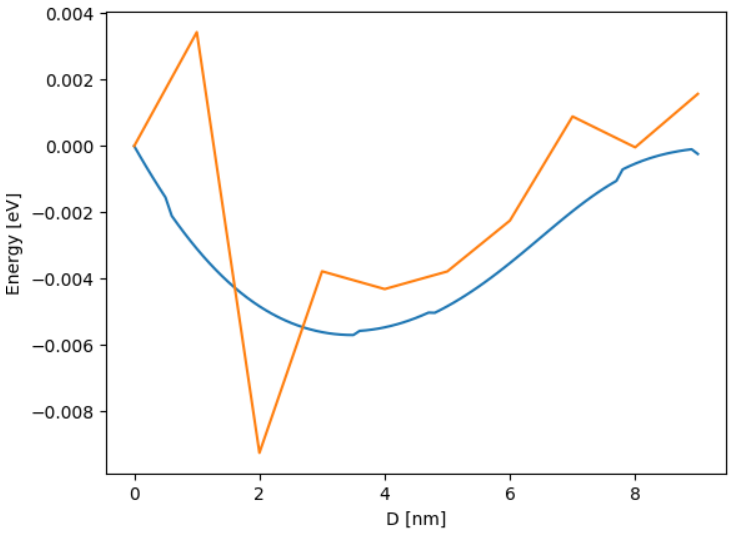

FIGURE 4.2: Comparison between the solutions of the linear method (in Blue) and the non-linear solutions (in Orange).

Figure 4.2 shows the results of the simulations in terms of the variation of energy ΔE for the ground state in terms of the overlap between the wires (measured by the distance D). For values of D larger than $4nm$ the points obtained using the linear and non-linear models are very close and follow the same trend. The main difference is a small decrease in the energy of the non-linear model, accounting for $\approx$ 20% of the variation of energy obtained by the linear model. On the other hand, for D smaller than $4nm$ there are significant differences between the results. In this case the two wires are strongly overlapped and basically they are equivalent to a single wire with two opposing corners cut out. Unfortunately, for the numerical method to account for the contributions of the electron distribution in the vicinity of these corners, it would require a very thin resolution of the discretisation grid used to calculate the finite differences associated with the Laplacian in Eq. 4.1. This exceeds the computational power available and therefore it is impossible

to validate the results for D smaller than $4nm$. Indeed, there are suspicions that the lack of computer power to resolve the cut out corners renders the numerical method unstable. This conjecture is further strengthened by the fact that the calculation for $D = 0nm$, where there is total overlap and there are no cut out corners, matches the energy values obtained when the two wires are strongly separated in both the linear and the non-linear models.

Clearly, solving the non-linear problem is quite difficult and the method developed needs to be improved to provide trustworthy results when the plasmonic structures have very thin details or, alternatively, requires an increase in the computer power available. However, the results obtained in the validity range of the numerical method strongly suggest that the non-linear terms produce a correction in the energy gaps of less than 20%, which is relatively small. This assessment needs to be confirmed by more in depth studies but for now it is possible to assume that the linear model provides a good estimate of the energy band gaps occurring in plasmonic nano-structures. The main advantage of using the linear model is that the calculations of the energy band gaps are tremendously faster and the numerical methods are much more stable.

4.3 Conclusions

This chapter analysed the importance of introducing the non-linear terms in the calculations. The preliminary results presented suggest, at least for small overlaps between the nano-wires and when the structure does not have thin details, that the non-linear terms introduce a relative small correction. In the case analysed, this corresponds to a small decrease in the energy band gap that produces a red shift of the absorption peak of real plasmonic structures relative to the predictions obtained by the linear models.

The next chapter will address the application of the properties of plasmons in metallic nano-structures to optical sensing.

Chapter 5

Towards Sensing Applications

The wide majority of the applications of plasmonics in sensing rely on the strong dependency of the absorption of surface plasmons on the optical properties of the materials at the metallic boundaries. These are in practice refractive index sensors. However, there have been recent proposals to use localized surface plasmons to directly measure other physical quantities aside refractive index [42]. This suggests that localized plasmons can be influenced by other physical quantities, and provide alternative approaches for sensing them.

This chapter discusses an example of application of the exotic properties of localized plasmons in nano-structures into sensing. This example is inspired by the results of chapter 3, where it was shown that the band gap of plasmonic modes in an artificial molecule composed of two nano-wires can be affected by an external electric field. This result can be used as a sensing principle for the detection and measurement of an electrostatic field.

The changes of the energy gap of the plasmons produced by the field modify the absorption spectrum of the nano-structures. In the development of an optical sensor it is not only necessary to have a dependency of the plasmons on the physical quantity, but also to interrogate these quantities with an optical field.

This chapter addresses both the design of the sensor and the description of the absorption of light by the plasmon modes associated with the interrogation process. The first section describes the sensor and shows how to model plasmons along a nano-wire in terms of the two dimensional dimer or plasmonic molecules described in the previous chapters. Subsequent sections discuss some of the performance characteristics of the sensor and a fabrication method that could be used to produce it.

5.1 Sensor Design and Operation

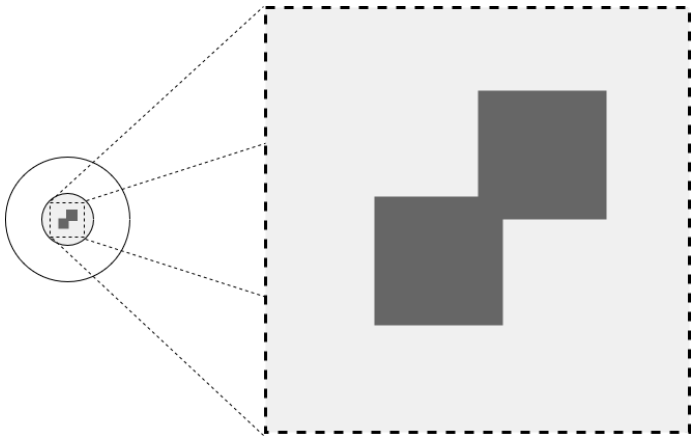

FIGURE 5.1: Geometry of the concept of sensor. The sensor is composed of two overlapping nano-wires with square cross section. Other choices in wire cross section are also possible although in this case a square helps to reduce the numerical error associated with the discretization of the representative grid.

The concept of the sensor consider two quantum wires at a close distance placed at the centre of the core of the fibre that work as an artificial diatomic molecule in the transverse section of the fibre. This is represented in Figure 5.1.

The cross section of the two nano-wires is very small and on its own would produce little effect on the optical field propagating on the fibre. However, the effects of plasmons accumulated over long propagation distances, resulting in measurable effects. To provide a full description of the interaction between the plasmons and the optical field, one begins by considering the three dimensional structure of the fibre and then reduce it to the two dimensional model described in the previous chapters.

The wave equation for an optical mode at the centre of the core of the fibre is approximatively given by

$$\partial_t^2 \vec{E} - v^2 \nabla^2 \vec{E} = \mu_0 \partial_t \vec{j} \tag{5.1}$$

where j is the current generated in the nano-wires as the plasmons oscillate between two modes. For simplicity the optical axis is along the z direction and it is assumed that the electric field distribution in each cross section of the fibre changes slowly, this means that

$$\partial_t^2 \vec{E} \approx i\omega \partial_t \vec{E} \tag{5.2}$$

where ω is the frequency of the optical field. Also, one may assume that

$$\vec{E}(x,y,z,t) = e^{i\beta z}\phi(x,y,t)\vec{u_E} \tag{5.3}$$

$$\vec{j}(x,y,z,t) = e^{i\beta z}\mathcal{J}(x,y,t)\vec{u_j} \tag{5.4}$$

which can be introduced in Eq. 5.1, yielding

$$i\partial_t\phi + \frac{v^2}{\omega}\beta^2\phi - \frac{v^2}{\omega}\nabla_\perp^2\phi = \frac{\mu_0}{\omega}\partial_t\mathcal{J} \tag{5.5}$$

where $\nabla_\perp$ is the Laplacian in the transverse direction.

On the other hand, the analogue Schrödinger equation for plasmons in the nano-wires can be written as

$$i\partial_t\psi + \frac{1}{2}\nabla^2\psi - V_{lin}\psi = \vec{\mu}\cdot\vec{E}\psi. \tag{5.6}$$

Then, introducing

$$\psi(x,y,z,t) = e^{i\beta z}\varphi(x,y,t), \tag{5.7}$$

it is possible to write

$$i\partial_t\varphi - \frac{1}{2}\beta^2\varphi + \frac{1}{2}\nabla_\perp^2\varphi - V_{lin}\varphi = \vec{\mu}\cdot\vec{E}\varphi. \tag{5.8}$$

Eq. 5.8 corresponds basically to the two dimensional physical model studied previously. In particular one has calculated functions of the form

$$\frac{1}{2}\nabla_\perp^2\varphi_n - V_{lin}\varphi_n = \mathcal{E}\varphi_n, \tag{5.9}$$

where φ_n are the quantum states corresponding to the plasmonic modes. So assuming that the field is tuned to the transition between two plasmon modes, the analogue wave finction can be written as

$$\varphi = C_a\varphi_a + C_b\varphi_b, \tag{5.10}$$

and it is possible to write Eq. 5.8 as

$$i\partial_t\begin{bmatrix}C_a\\C_b\end{bmatrix} - \frac{1}{2}\beta^2\begin{bmatrix}C_a\\C_b\end{bmatrix} + \begin{bmatrix}\mathcal{E}_a & 0\\0 & \mathcal{E}_b\end{bmatrix}\begin{bmatrix}C_a\\C_b\end{bmatrix} = \begin{bmatrix}\Omega_{AA}(t) & \Omega_{AB}(t)\\\Omega_{BA}(t) & \Omega_{BB}(t)\end{bmatrix}\begin{bmatrix}C_a\\C_b\end{bmatrix}. \tag{5.11}$$

Now we define the effective Rabi frequencies as

$$\Omega'_{AA}(t) = \Omega_{AA}(t) - \frac{1}{2}\beta^2 + \mathcal{E}_a \tag{5.12}$$

$$\Omega'_{BB}(t) = \Omega_{BB}(t) - \frac{1}{2}\beta^2 + \mathcal{E}_b \tag{5.13}$$

such that

$$\partial_t \begin{bmatrix} C_a \\ C_b \end{bmatrix} = -i \begin{bmatrix} \Omega_{AA}(t) & \Omega_{AB}(t) \\ \Omega_{BA}(t) & \Omega_{BB}(t) \end{bmatrix} \begin{bmatrix} C_a \\ C_b \end{bmatrix}, \tag{5.14}$$

This result is formally analogue to the Bloch equations derived in the context of the semi-classical model for the interaction of a two level atom with a resonant or near resonant electromagnetic field. With this derivation we further strengthen the analogy between the interaction of light with nano-wires supporting localized plasmons. The solution of this equation follows then the standard approach developed in the context of Quantum Optics to describe the absorption of light by an atom and a consequent excitation of the ground state into higher energy states.

If the electromagnetic field is coherent, it is possible for the plasmons and the field to exchange energy as they propagate along the fibre, giving rise to a phenomena known as Rabi oscillations, which strongly depends on the detuning between the field and the energy gap of the plasmon modes.

To calculate the absorption coefficient of the plasmons, one begins by recasting Eq. 5.14 in the interaction picture, obtaining [43]

$$\partial_t \begin{bmatrix} C_a \\ C_b \end{bmatrix} = -i \begin{bmatrix} 0 & \Omega(t) \\ \Omega^*(t) & 0 \end{bmatrix} \begin{bmatrix} C_a \\ C_b \end{bmatrix}, \tag{5.15}$$

with $\Omega(t) \equiv \Omega_{A,B}$.

If one now applies the rotating wave approximation, $\Omega(t)$ takes the form

$$\Omega(t) \approx \frac{\Omega_0}{2} e^{i(\omega-\omega_0)t} = \frac{\Omega_0}{2} e^{i\Delta t}, \tag{5.16}$$

where $\Delta = (\omega - \omega_0)$ and is defined as the detuning between the field frequency ω_0 and the natural frequency of the transition of the energy levels ω.

This implies that

$$|C_b(t)|^2 = \frac{\Omega_0^2}{\Omega'^2} \sin^2\left(\frac{\Omega' t}{2}\right), \tag{5.17}$$

where $\Omega' = \sqrt{\Omega_0^2 + \Delta^2}$.

The change in the state of the atom corresponds to a change in the plasmon mode of the nano-structure, resulting in a change of the charge distribution and ultimately in a small current. In practice, the plasmonic structure acts as a small antena which absorbs and re-emits light. This absorption and re-emission of light is proportional to $|C_b(t)|^2$ that

corresponds to the probability of exciting the system to $|B\rangle$ and, in doing so, absorbing photons.

These result show that the Rabi oscillations are strongly dependent on the energy gap between the two energy levels of an atom. As shown in chapter 2 the sensor works as an artificial diatomic molecule in the transverse cross section of the fibre (see Figure 5.1). The energy levels of this artificial molecule can be Stark shifted by an applied static electric field that promotes the de-localization of the free electrons. As a result, the light propagating in the fibre excites the Rabi oscillations between plasmonic levels whose frequency strongly depends on the amplitude of the static electric field along the molecular axis. As it was presented in section 2.3 and chapter 3, it is possible to develop a semi-classical description of the plasmonic modes of the system following the Hydrodynamical Drude model in association with the Madelung formalism.

Figure 5.2 presents the energy levels of the first four eigenstates in function of the distance D for different values of $\vec{E}$. By analysing this figure one can clearly see the Stark effect, as the energy of each level increases with the electric field. Another important feature in Figure 5.2 is the degeneracy splitting in the region of $D > 8nm$ for higher values of $|\vec{E}|$.

These results strengthen the analogy between plasmonic modes and the molecular orbitals resulting from the chemical bond of two atoms. As shown, the energy bands of the analogue system can be affected by an external electric field resulting in a Stark effect and in splitting of the degeneracy for values of D larger than $8nm$, when considering this structure, which implies that the sensor would be more sensible to the effects of an applied electric field with that geometry, as the Rabi oscillations depend strongly on the band gap between two levels.

Figure 5.3 presents the dependency of the energy gap of the first two levels with the applied electrostatic field for different values of θ with $D = 8nm$. The blue line represents the energy gap between the two levels in function of the applied electrostatic field for $D = 8nm$ and $\theta = \frac{\pi}{4}$ while the orange line shows for $D = 8nm$ and $\theta = 0$. This figure clearly shows the dependency of the system on the electric field direction if the symmetry of the system is broken. Analysing this figure, one can also infer about the sensitivity of the sensor meaning that for values of $\theta = \pi/4$ the sensitivity is $1.065\frac{eV}{V/m}$ and for $\theta = 0$ is $0.781667\frac{eV}{V/m}$.

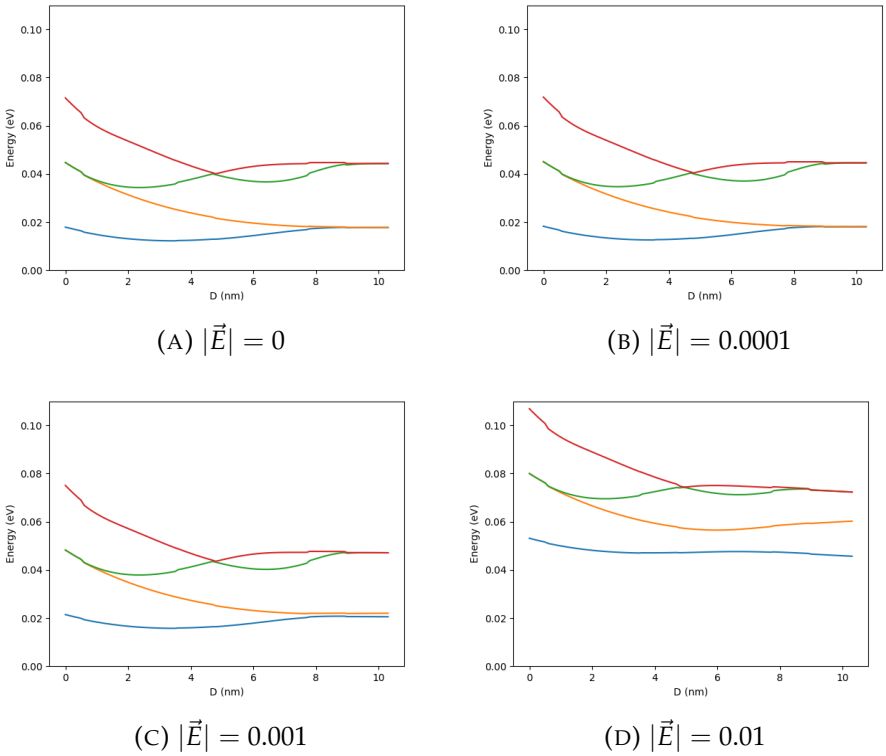

(A) $|\vec{E}| = 0$ (B) $|\vec{E}| = 0.0001$

(C) $|\vec{E}| = 0.001$ (D) $|\vec{E}| = 0.01$

FIGURE 5.2: Energy levels of the first 4 states for different $\vec{E}$ with $\theta = \pi/4$. This figure shows the interplay between the geometry of the nano-wires (expressed in terms of the separation between the wires, D) and the amplitude of the electric field in determining the energy gaps between the plasmonic modes and therefore, the resonant frequency of light absorbed by the wires. Using this information. it is possible to design nano-wire structures with absorption peaks at specific optical ranges for a wide range of electric field amplitude.

In contrast to Figure 5.3, Figure 5.4 shows the energy gap for values of $D = 4nm$, where in blue is represented the values for $\theta = \frac{\pi}{4}$ and in orange for $\theta = 0$. The sensitivity achieved for values of $\theta = \frac{\pi}{4}$ is $0.26833 \frac{eV}{V/m}$ whereas for values of $\theta = 0$ is $0.145833 \frac{eV}{V/m}$.

As expected with this geometry, the sensor has the best sensitivity for $D = 8nm$ and $\theta = \frac{\pi}{4}$. Another important feature is that the sensor is responsive to different values of θ and highly dependant of the geometry as one can see comparing both Figures 5.3 and 5.4. Finally, if one looks to the values of the energy gap one notices that the wavelength associated with them is around tens of micrometres. Configuration can not be directly applied as a fibre optic sensor however, one could rectify this by changing the geometry to impose that the energy gap lies around $1 \approx 2eV$ so that the wavelength of the electromagnetic field would be placed in the visible spectrum or near infra-red.

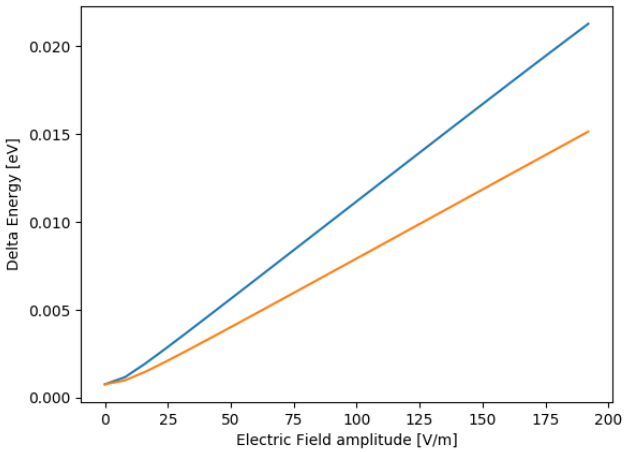

FIGURE 5.3: Difference of energy of the two first levels in order of electrostatic field for different values of θ with the separation $D = 8nm$. The Blue line represents the values for $\theta = \frac{\pi}{4}$ and the orange for$\theta = 0$.

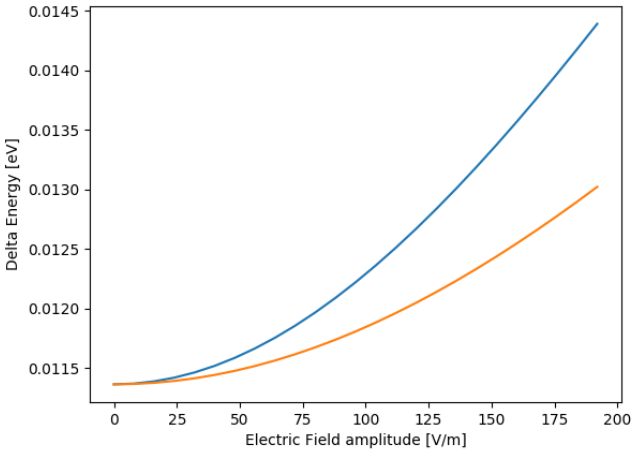

FIGURE 5.4: Difference of energy of the two first levels in order of electrostatic field for different values of θ with the separation $D = 4nm$. The Blue line represents the values for $\theta = \frac{\pi}{4}$ and the orange for$\theta = 0$.

5.2 Fabrication Techniques

The sensor theorized in this chapter is based on a fibre optics where two silver nano-wires are placed in the centre of the core. However, this kind of fibre optics is not commonly seen and this section discusses a possible viable procedure to fabricate it.

One of the techniques used to produce fibre optics is the modified chemical vapour deposition. In this technique a hollow cylinder of silicon is placed in rotation. In the centre of the cylinder flows pure oxygen and, in the particular case of doped fibre, a mixture of pure oxygen and the doping reactants. A mobile heat source keeps the cylinder at 1500^oC.

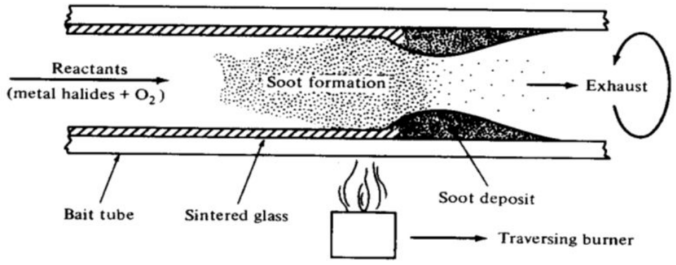

FIGURE 5.5: The first step of the fabrication of a fibre optic.

At these temperatures the oxygen enters in contact with the inner walls of the cylinder thus creating a thin layer of highly pure silica. A representation of this step can be seen in Figure 5.5.

The cylinder with the thin layer of silica, which is called the pre-form, if the objective was to fabricate a normal fibre optic, the pre-form is heated to around 2000^oC and is collapsed. After the collapse the thin layer of silicon is the core of the fibre and the rest of the silica is the cladding. After this process the pre-form has generally $10 - 25mm$ and can reach to $1m$ long. However, in this particular case, an additional step is needed. When the pre-form is fabricated one can introduce the silver in the position and geometry needed. Since at these temperatures, the silver is in a liquid state, it will flow and fill the space available thus forming the nano-wires desired.

5.3 Conclusions

Nano-plasmonics is a new field of research with the tremendous potential of applications and optical sensors constitute a key enabling technology, not only due to its impact on monitoring technologies, but also as a test bed to understand better the behaviour of plasmons at the scales of a few atoms. As shown in this chapter, plasmonics can be used to develop nano-resonators that act as artificial molecules, that can be used to evaluate the electric field. This approach is still in the beginning but the preliminary results suggest that a new generation of sensors could result from further development of these ideas.

.

Chapter 6

Concluding remarks and future work

This thesis is dedicated to the study of the properties of plasmons at the nano-scale and how they differ from their properties in the bulk of materials or at the interface between metal and dielectrics. Clearly the collective oscillations of free charges in one or more dimensions dramatically alter the optical properties of metals. If one confines plasmons in two dimensions to scales down to a few nanometres, like in the case of a nano-wire, quantum effects start to arise. The sheer confinement produces large energy gaps between the plasmons modes which corresponds to frequencies in the optical or near optical range. This can be interesting for a diversity of applications, that include optical sensing.

As plasmons become confined to shorter scales, effects such as quantum tunnelling, coherence and quantum entanglement become possible, as shown by a wide variety of experiments. These too can have tremendous technological applications. However, at these scales the nature of plasmons and photon-plasmon interaction still poses a challenge, both from the conceptual and experimental perspective. As shown in this dissertation, modelling plasmons in nano-structures poses many difficulties, not only due to their complexity and dependence on geometry, but also due to intrinsic non-linearities. As a result, standard analyses and modern techniques can only provide a first approximation or even fail completely.

In this dissertation one identifies many of these aspects and provides methodological approaches to address them. In particular, we have incorporated quantum effects, such as the Thomas-Fermi potential associated with the Pauli exclusion principle, in the hydrodynamical Drude model and converted it into an analogue quantum problem which captures not only these, but also the energy gaps of the plasmon modes.

This model also allowed the development of computational methods that tackle this challenging problems. Furnished with these tools, one can explore potential technological applications in particular the proposed electrostatic field sensor based on fibre optics and plasmonic. Unlike common plasmonic sensors, this one doesn't rely on the change of refractive index produced by the electric field. The sensor design is composed by two nano-wires embedded in the core of an optical fibre which can absorb light over different wavelengths depending on the field.

These results are but the conceptual proof of principle and the new phenomena of nano-plasmonics promises a future with formidable technological breakthroughs.

Appendix A

The Madelung Formalism

The motion of electrons in a metal, under the influence of an electromagnetic field, can be described according to the hydrodynamical Drude model by the fluid equations:

$$-\partial_t n = \nabla \cdot (n\vec{u}) \tag{A.1}$$

$$n\partial_t \vec{u} + n(\vec{v}\cdot\nabla)\vec{u} = -\frac{ne}{m_e}(\vec{E} + \vec{u}\times\vec{B}) - \frac{\nabla P}{m_e} - \gamma n\vec{u}. \tag{A.2}$$

The Madelung Formalism was initially established to re-express the Schrödinger equation in terms of the fluid equations that describe the flow of probability of the wave-function in quantum systems. The Schrödinger equation is then

$$i\hbar\alpha\partial_t\psi = \left[-\frac{\hbar^2\beta}{2m}\nabla^2 + V\right]\psi, \tag{A.3}$$

where α and β are normalising constants in order to transform Eq. A.3 into Eqs. A.1 and A.2, it is also necessary to assume that the solution to this Schrödinger equation takes the form of $\psi = n^{1/2}e^{i\mathcal{S}}$. Which implies that

$$\partial_t\psi = \frac{1}{2}\frac{\dot{n}}{n^{1/2}}e^{i\mathcal{S}} + i\dot{\mathcal{S}}n^{1/2}e^{i\mathcal{S}} \tag{A.4}$$

and

$$\nabla^2\psi = (\partial_x^2 + \partial_y^2)\psi, \tag{A.5}$$

where

$$\partial\psi = \frac{1}{2}\frac{\partial_x}{n^{1/2}}e^{i\mathcal{S}} + i\partial_x\mathcal{S}n^{1/2}e^{i\mathcal{S}} = n^{1/2}e^{i\mathcal{S}}\left(i\partial_x\mathcal{S} + \frac{\partial_x n}{2n}\right) \tag{A.6}$$

which leads to:

$$\partial_x^2\psi = \left[\frac{1}{2}\frac{\partial_x^2 n}{n} - \frac{1}{2}\left(\frac{\partial_x n}{n}\right)^2 + i\partial_x^2\mathcal{S}\right] n^{1/2}e^{i\mathcal{S}} + \left(\frac{1}{2}\frac{\partial_x n}{n} + i\partial_x\mathcal{S}\right) n^{1/2}e^{i\mathcal{S}}. \tag{A.7}$$

Applying the same method to $\partial_y^2\psi$, then

$$\nabla^2\psi = \left[\frac{1}{2}\frac{\nabla^2 n}{n} - \frac{1}{4}\frac{\nabla n^2}{n} - (\nabla\mathcal{S})^2 + i\nabla^2\mathcal{S} + i\frac{\nabla n\nabla\mathcal{S}}{n}\right] n^{1/2}e^{i\mathcal{S}}. \tag{A.8}$$

Replacing Eq. A.4 and Eq. A.8 in Eq. A.3 and deviding it in two sets of equations, one with the imaginary part and the other with the real part, one has:

$$\frac{\hbar\alpha}{2}\dot{n} = \left[-\frac{\hbar^2\beta}{2m}\left(\nabla^2\mathcal{S} + \frac{\nabla n\nabla\mathcal{S}}{n}\right)\right] n \tag{A.9}$$

for the imaginary part, and

$$-\hbar\alpha\dot{\mathcal{S}} = -\frac{\hbar^2\beta}{2m}\left[\frac{1}{2}\frac{\nabla^2 n}{n} - \frac{1}{4}\left(\frac{\nabla n}{n}\right)^2 - (\nabla\mathcal{S})^2\right] + V \tag{A.10}$$

for the real part.

Defining $\nabla\mathcal{S} = u$ then Eq. A.9 transforms into

$$\dot{n} = -\frac{\beta}{\alpha}\frac{\hbar}{m}\nabla\cdot(nu), \tag{A.11}$$

comparing to Eq. A.1 means that

$$\frac{\beta}{\alpha}\frac{\hbar}{m} = 1. \tag{A.12}$$

From Eq. A.10, one has:

$$-\dot{\mathcal{S}} = -\frac{\beta}{\alpha}\frac{\hbar}{2m}\left[\frac{1}{2}\frac{\nabla^2 n}{n} - \frac{1}{4}\left(\frac{\nabla n}{n}\right)^2 - (\nabla\mathcal{S})^2\right] + \frac{1}{\alpha\hbar}V \tag{A.13}$$

defining $V = V' - \beta V_B$, where

$$V_B = -\frac{\hbar^2}{4m}\left[\frac{\nabla^2 n}{n} - \frac{1}{2}\left(\frac{\nabla n}{n}\right)^2\right] = -\frac{\hbar^2}{4m}\frac{\nabla^2\sqrt{n}}{\sqrt{n}} \tag{A.14}$$

is the Bohm Potential.

With this in mind, Eq. A.13 simplifies to:

$$-\dot{\mathcal{S}} = \frac{\beta}{\alpha}\frac{\hbar}{2m}(\nabla\mathcal{S})^2 + \frac{V'}{\alpha\hbar}. \tag{A.15}$$

Again, by defining $\nabla \mathcal{S} = u$, one has:

$$-\dot{u} = \frac{\beta}{\alpha}\frac{\hbar}{2m}\nabla(u \cdot u) + \frac{1}{\alpha\hbar}\nabla V' \tag{A.16}$$

and, as $\nabla(u \cdot u) = 2(u \cdot \nabla)u$, Eq A.16 transforms into

$$-\dot{u} = \frac{\beta}{\alpha}\frac{\hbar}{m}(u \cdot \nabla)u + \frac{1}{\alpha\hbar}\nabla V'. \tag{A.17}$$

For this equation to be equal to Eq. A.2, one finds again the condition

$$\frac{\beta}{\alpha}\frac{\hbar}{m} = 1. \tag{A.18}$$

Rearranging Eq. A.17, one reaches to:

$$n\vec{u} + n(\vec{u} \cdot \nabla)\vec{u} = -\frac{m}{\beta\hbar^2}n\nabla V'. \tag{A.19}$$

Therefore, one has:

$$\nabla V' = \frac{\beta\hbar^2 e}{m^2}\left[\vec{E} + \vec{u} \times \vec{B}\right] + \frac{\beta\hbar^2}{m^2}\frac{1}{n}\nabla P + \gamma\frac{\beta\hbar^2}{m}\vec{u} + \frac{\beta\hbar^2}{m^2}\nabla\mathcal{U}, \tag{A.20}$$

where $\vec{E}$ is the electric field, $\vec{B}$ is the magnetic field, P is the Thomas-Fermi pressure, γ losses coefficient and $\mathcal{U}$ the confining potential.

One should note that

$$\frac{1}{n}\nabla P = \frac{1}{n}\nabla((3\pi^2)^{2/3}\frac{h^2}{5m}n^{5/3}) = \frac{(3\pi^2)^{2/3}h^2}{5m}\frac{1}{n}\nabla n^{5/3}, \tag{A.21}$$

as

$$\begin{aligned} \tfrac{1}{n}\nabla n^{5/3} &= \tfrac{5}{3n}n^{2/3}\nabla n \\ &= \tfrac{5}{3}n^{-1/3}\nabla n \\ &= \tfrac{5}{2}\nabla n^{2/3}. \end{aligned} \tag{A.22}$$

As the magnetic field in an electromagnetic wave is small when compared its electric field and as our model has yet to consider losses, the potential V takes the form:

$$V = \frac{\beta\hbar^2 e}{m^2}\vec{r} \cdot \vec{E} + \frac{\beta\hbar^2}{m^2}\frac{(3\pi^2)^{2/3}h^2}{2m}n^{2/3} + \frac{\beta\hbar^2}{m^2}\mathcal{U} + \beta\frac{\hbar^2}{4m}\frac{\nabla^2\sqrt{n}}{\sqrt{n}}. \tag{A.23}$$

The definition $\psi = n^{1/2}e^{i\mathcal{S}}$ implies that $n = n_0|\psi|^2$ which means that

$$V = \frac{\beta\hbar^2 e}{m^2}\vec{r}\cdot\vec{E} + \frac{\beta\hbar^2}{m^2}\frac{(3\pi^2)^{2/3}h^2N^{2/3}}{2m}|\psi|^{4/3} + \frac{\beta\hbar^2 e}{m^2}\mathcal{U}[eV] + \beta\frac{\hbar^2}{4m}\frac{\nabla^2\sqrt{|\psi|^2}}{\sqrt{|\psi|^2}}. \tag{A.24}$$

With this one can now re-express Eqs. 2.74 and 2.75 into a non-linear Schrödinger equation where the potential takes the form of Eq. A.24.

Bibliography

[1] *Surface plasmon resurrection*, Nature Photonics **6** (2012), 10.1038/nphoton.2012.296.

[2] E.-P. Li and H.-S. Chu, *Plasmonic Nanoelectronics and Sensing*, 1st ed. (Cambridge University Press, 2014).

[3] M. Rezaei, P. Rasekh, and R. Safian, *A Stripe Assisted Hybrid Palsmonic Waveguide for the Propagation of Terahertz Waves*, IEEE Photonics Technology Letters (2015), 10.1109/lpt.2015.2461636.

[4] E. Ozbay, *Plasmonics: Merging Photonics and Electronics at Nanoscale Dimensions*, Science **311** (2006), 10.1126/science.1114849.

[5] W. L. Barnes, A. Dereux, and T. W. Ebbesen, *Surface plasmon subwavelength optics*, Nature **424** (2003), 10.1038/nature01937.

[6] A. Rider, K. Ostrikov, and S. Furman, *Plasmas meet Plasmonics*, The European Physical Journal D (2012).

[7] K. L. Ngai, E. N. Economou, and M. H. Cohen, *Theory of Inelastic Electron-Surface-Plasmon Interactions in Metal-Semiconductor Tunnel Junctions*, Physical Review Letters **22** (1969), 10.1103/PhysRevLett.22.1375.

[8] M. Kauranen and A. V. Zayats, *Nonlinear plasmonics*, Nature Photonics **6** (2012), 10.1038/nphoton.2012.244.

[9] A. V. Zayats, I. I. Smolyaninov, and A. A. Maradudin, *Nano-optics of surface plasmon polaritons*, Physics Reports **408** (2005), 10.1016/j.physrep.2004.11.001.

[10] J. H. e. Jiří Homola (auth.), *Surface plasmon resonance based sensors*, 1st ed., Springer Series on Chemical Sensors and Biosensors 4 (Springer-Verlag Berlin Heidelberg, 2006).

[11] Y. Wang, E. W. Plummer, and K. Kempa, *Foundations of Plasmonics*, Advances In Physics **60** (2011), 10.1080/00018732.2011.621320.

[12] S. Zeng, X. Yu, W.-C. Law, Y. Zhang, *et al.*, *Size dependence of Au NP-enhanced surface plasmon resonance based on differential phase measurement*, Sensors and Actuators B: Chemical **176** (2013), 10.1016/j.snb.2012.09.073.

[13] H. Moayyed, I. T. Leite, L. Coelho, J. L. Santos, and D. Viegas, *Analysis of Phase Interrogated SPR Fiber Optic Sensors With Bimetallic Layers*, IEEE Sensors Journal **14** (2014), 10.1109/JSEN.2014.2329918.

[14] T. G. D. E. E. T. W. L. H. J. Ghaemi, H. F.; Thio, *Surface plasmons enhance optical transmission through subwavelength holes*, Physical Review B **58** (1998), 10.1103/physrevb.58.6779.

[15] A. Ovsianikov, B. N. Chichkov, A. I. Kuznetsov, A. B. Evlyukhin, *et al.*, *Laser-induced transfer of metallic nanodroplets for plasmonics and metamaterial applications*, Journal of the Optical Society of America B **26** (2009), 10.1364/JOSAB.26.00B130.

[16] D. N. Mermin and N. W. Ashcroft, *Solid State Physics*, college ed., edited by D. Crane (CRC Press, 1976) pp. 1–27.

[17] H. Horvath, *Gustav Mie and the scattering and absorption of light by particles: Historic developments and basics*, Journal of Quantitative Spectroscopy and Radiative Transfer (2009), 10.1016/j.jqsrt.2009.02.022.

[18] E. Hutter and J. Fendler, *Exploitation of Localized Surface Plasmon Resonance*, Advanced Materials **16** (2004), 10.1002/adma.200400271.

[19] C. Ciracì, J. B. Pendry, and D. R. Smith, *Hydrodynamic Model for Plasmonics: A Macroscopic Approach to a Microscopic Problem*, ChemPhysChem **14**, 1109 (2013).

[20] A. Eguiluz and J. J. Quinn, *Hydrodynamic model for surface plasmons in metals and degenerate semiconductors*, Physical Review B **14** (1976), 10.1103/physrevb.14.1347.

[21] C. Ciraci, R. T. Hill, J. J. Mock, Y. Urzhumov, *et al.*, *Probing the Ultimate Limits of Plasmonic Enhancement*, Science **337** (2012), 10.1126/science.1224823.

[22] G. Martino, Y. Sonnefraud, S. Kéna-Cohen, M. Tame, Şahin K. Özdemir, M. S. Kim, and S. A. Maier, *Quantum Statistics of Surface Plasmon Polaritons in Metallic Stripe Waveguides*, NANOLetters **12**, 2504 (2013).

[23] M. S. Tame, K. R. McEnery, . K. Özdemir, J. Lee, S. A. Maier, and M. S. Kim, *Quantum plasmonics*, Nature Physics **9**, 329 (2012).

[24] e. a. Paul Kwiat, *New High-Intensity Source of Polarization-Entangled Photon Pairs*, Physical Review Letters **75**, 4337 (1995).

[25] R. Esteban, A. G. Borisov, P. Nordlander, and J. Aizpurua, *Bridging quantum and classical plasmonics with a quantum-corrected model*, Nature Communications **3**, 825 (2012).

[26] D. C.Marinica, A. K. Kazansky, P. Nordlander, J. Aizpurua, and A. G. Borisov, *Quantum Plasmonics: Nonlinear Effects in the Field Enhancement of a Plasmonic Nanoparticle Dimer*, Nature Communications **3**, 825 (2012).

[27] D. C.Marinica, A. K. Kazansky, P. Nordlander, J. Aizpurua, and A. G. Borisov, *A comparison of graphene, superconductors and metals as conductors for metamaterials and plasmonics*, Nature Communications **3**, 825 (2012).

[28] E. Altewischer, M. P. van Exter, and J. P. Woerdman, *Plasmon-assisted transmission of entangled photons*, Nature **418** (2002), 10.1038/nature00869.

[29] M. S. Tame, C. Lee, J. Lee, D. Ballester, M. Paternostro, A. V. Zayats, and M. S. Kim, *Single-Photon Excitation of Surface Plasmon Polaritons*, Physical Review Letters **101** (2008), 10.1103/PhysRevLett.101.190504.

[30] J. Takahara, F. Kusunoki, T. Kobayashi, S. Kawata, V. M. Shalaev, and D. P. Tsai (2005).

[31] G. Giuliani and G. Vignale, *Quantum Theory of the Electron Liquid*, 1st ed. (Cambridge University Press, 2005).

[32] D. F. P. Pile, T.Ogawa, D. K. Gramotnev, Y.Matsuzaki, *et al.*, *Two-dimensionally localized modes of a nanoscale gap plasmon waveguide*, Applied Physics Letters **87** (2005), 10.1063/1.2149971.

[33] J. Bochterle, F. Neubrech, T. Nagao, and A. Pucci, *Angstrom-Scale Distance Dependence of Antenna-Enhanced Vibrational Signals*, ACS Nano (2012), 10.1021/nn304341c.

[34] A. Liu, G. Abbineni, and C. Mao, *Nanocomposite Films Assembled from Genetically Engineered Filamentous Viruses and Gold Nanoparticles: Nanoarchitecture- and*

Humidity-Tunable Surface Plasmon Resonance Spectra, Advanced Materials **21** (2009), 10.1002/adma.200800777.

[35] C. M. Cobley, S. E. Skrabalak, D. J. Campbell, and Y. Xia, *Shape-Controlled Synthesis of Silver Nanoparticles for Plasmonic and Sensing Applications*, Plasmonics **4** (2009), 10.1007/s11468-009-9088-0.

[36] Y. Shen, J. Zhou, T. Liu, Y. Tao, *et al.*, *Plasmonic gold mushroom arrays with refractive index sensing figures of merit approaching the theoretical limit*, Nature Communications **4** (2013), 10.1038/ncomms3381.

[37] C. Jeppesen, A. Kristensen, S. Xiao, and N. A. Mortensen, *Metamaterial localized resonance sensors: prospects and limitations*, Optics Express **18** (2010), 10.1364/OE.18.025075.

[38] J.-M. Liu, *Photonic Devices*, 1st ed. (Cambridge University Press, 2005).

[39] L. E.-P. and C. H.-S. (eds.), *Plasmonic Nanoelectronics and Sensing*, EuMA High Frequency Technologies Series (Cambridge University Press, 2014).

[40] A. Eguiluz and J. J. Quinn, *Hydrodynamic model for surface plasmons in metals and degenerate semiconductors*, Physical Review B **14**, 1347 (1976).

[41] E. Madelung, *Eine anschauliche Deutung der Gleichung von Schrödinger*, Naturwissenschaften (The Science of Nature) **14**, 1004 (1926).

[42] D. F. Santos, A. Guerreiro, and J. M. Baptista, *Simultaneous Plasmonic Measurement of Refractive Index and Temperature Based on a D-Type Fiber Sensor With Gold Wires*, IEEE Sensors Journal **17** (2017), 10.1109/JSEN.2017.2674522.

[43] *Introductory Quantum Optics*.